

## 18. ROCK MAGNETIC IDENTIFICATION OF MAGNETIC IRON SULFIDES AND ITS BEARING ON THE OCCURRENCE OF GAS HYDRATES, ODP LEG 204 (HYDRATE RIDGE)<sup>1</sup>

Juan Cruz Larrasoña,<sup>2</sup> Eulàlia Gràcia,<sup>3</sup> Miguel Garcés,<sup>4</sup>  
Robert J. Musgrave,<sup>5</sup> Elena Piñero,<sup>3</sup> Francisca Martínez-Ruiz,<sup>6</sup>  
and Marta E. Vega<sup>7</sup>

### ABSTRACT

In this paper, we present a rock magnetic data set produced for sediments from Hydrate Ridge recovered during Ocean Drilling Program Leg 204. Our data set is based on several artificially induced magnetic properties that can be used as a diagnostic for the presence of magnetic iron sulfides. The occurrence of magnetic iron sulfides within the gas hydrate stability zone in locations where gas hydrates are present seems to confirm previous interpretations linking formation of such minerals with generation of gas hydrate. Magnetic iron sulfides are also found at positions deeper than the gas hydrate stability zone. We suggest that these positions, which include intervals located just below the bottom-simulating reflector and also at deeper positions, may mark the former presence of gas hydrates that have been later dissociated as the gas hydrate stability zone moved upward through time. Detailed characterization of the magnetic iron sulfide mineralogy and comparison with sedimentological and geochemical data will be attempted for better determining the significance of magnetic iron sulfides in Hydrate Ridge sediments and their possible applications in the study of gas hydrates.

<sup>1</sup>Larrasoña, J.C., Gràcia, E., Garcés, M., Musgrave, R.J., Piñero, E., Martínez-Ruiz, F., and Vega, M.E., 2006. Rock magnetic identification of magnetic iron sulfides and its bearing on the occurrence of gas hydrates, ODP Leg 204 (Hydrate Ridge). In Tréhu, A.M., Bohrmann, G., Torres, M.E., and Colwell, F.S. (Eds.), *Proc. ODP, Sci. Results*, 204, 1–33 [Online]. Available from World Wide Web: <[http://www-odp.tamu.edu/publications/204\\_SR/VOLUME/CHAPTERS/111.PDF](http://www-odp.tamu.edu/publications/204_SR/VOLUME/CHAPTERS/111.PDF)>. [Cited YYYY-MM-DD]

<sup>2</sup>Departamento de Ciencias de la Tierra, Universidad de Zaragoza, 50009 Zaragoza, Spain. [jclarra@unizar.es](mailto:jclarra@unizar.es)

<sup>3</sup>Unitat de Tecnologia Marina, Centre Mediterrani d'Investigacions Marines i Ambientals—CSIC, 08003 Barcelona, Spain.

<sup>4</sup>Group of Geodynamics and Basin Analyses, University of Barcelona, 08028 Barcelona, Spain.

<sup>5</sup>School of Geosciences, Monash University, Clayton VIC 8000, Australia.

<sup>6</sup>Instituto Andaluz de Ciencias de la Tierra (CSIC)—Universidad de Granada, 18002 Granada, Spain.

<sup>7</sup>PALM Laboratory, La Trobe University, Bundoora VIC 3086, Australia.

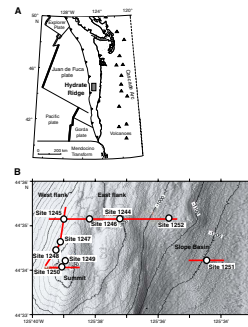
## INTRODUCTION

Hydrate Ridge is a structural high located in the accretionary complex of the Cascadia subduction zone, offshore Oregon (USA) (Fig. F1). During Ocean Drilling Program Leg 204, nine sites were drilled throughout the southern sector of Hydrate Ridge (Tréhu, Bohrmann, Rack, Torres, et al., 2003), where a ubiquitous bottom-simulating reflector (BSR), geophysical and geochemical data, and direct recovery evidence widespread distribution of gas hydrates in the sediments (Tréhu et al., 1999, 2004b; Tréhu, Bohrmann, Rack, Torres, et al., 2003). A line-drawing of high-resolution three-dimensional multichannel seismic (MCS) reflection data available during Leg 204 (Tréhu et al., 2002) illustrates the main stratigraphic and structural features of Hydrate Ridge as well as the relationship between characteristic reflectors (Fig. F2). The sedimentary sequence that builds southern Hydrate Ridge has been divided into five lithostratigraphic units that range from early Pleistocene to Holocene in age (Tréhu, Bohrmann, Rack, Torres, et al., 2003). Beneath these units, older sediments constituting the accretionary prism of the subduction zone are located (Tréhu, Bohrmann, Rack, Torres, et al., 2003). Hydrate Ridge sediments, including those in the accretionary complex, are mainly composed of hemipelagic clays and silty clays that are locally interbedded by silty- to sandy-rich turbidite levels that often contain volcanic ash and glass (Shipboard Scientific Party, 2003; Gracia et al., this volume). Hemipelagic clays and silty clays often show a mottled pattern related with the ubiquitous presence of variable amounts of black, millimeter-scale iron sulfide nodules (Shipboard Scientific Party, 2003). On some occasions, iron sulfides are found as larger nodules (up to 1 cm) that are strongly magnetic (Shipboard Scientific Party, 2003). Silty- to sandy-rich turbidite layers especially cluster around three specific intervals that constitute characteristic seismic reflectors labeled as Horizons A, B, and B' (Tréhu, Bohrmann, Rack, Torres, et al., 2003; Shipboard Scientific Party, 2003). Horizon A has been suggested to be a conduit feeding gas from the deep accretionary complex sediments to the surface vents and gas hydrate deposits (Tréhu et al., 2004a). In the slope basin, two large debris flows composed of unsorted pebble-size mud clasts embedded in a clay matrix and affected by soft-sediment deformation structures are intercalated in the hemipelagic clays and silty clays (Fig. F2) (Shipboard Scientific Party, 2003).

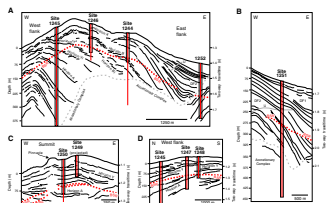
Previous rock magnetic results from Hydrate Ridge sediments have shown a widespread occurrence of magnetic iron sulfides, predominantly greigite but probably also pyrrhotite, associated with gas hydrates (Housen and Musgrave, 1996). Moreover, a number of studies have reported the occurrence of greigite related to anaerobic oxidation of methane (e.g., Kasten et al., 1998; Neretin et al., 2004). Because the occurrence of greigite and pyrrhotite can be related to formation of gas hydrates and degradation of methane, identification of magnetic iron sulfides may have implications for understanding the processes that control formation and accumulation of methane and gas hydrates in marine sediments. Greigite and pyrrhotite can survive through geological time (e.g., Verosub and Roberts, 1995). Thus, identification of these magnetic iron sulfides might also have implications for understanding methane- and gas hydrate-bearing marine sediments in ancient sedimentary systems.

Identification of magnetic iron sulfides in sediments can be achieved using geochemical analyses (e.g., Neretin et al., 2004) and mineralogical

F1. Cascadia accretionary margin, p. 10.



F2. Line-drawings of Hydrate Ridge, p. 11.



techniques such as X-ray diffraction (XRD) and scanning electron microscopy (SEM) (e.g., Horng et al., 1998; Roberts and Weaver, 2005). Magnetic methods also provide an excellent tool for identifying magnetic iron sulfides because they are very sensitive to the very low concentrations that often hamper identification of magnetic iron sulfides by means of conventional geochemical and mineralogical techniques. Identification of magnetic iron sulfides in Hydrate Ridge sediments has been mostly based on magnetic parameters derived from hysteresis experiments (Housen and Musgrave, 1996). However, such experiments require specific equipment that is not available in most paleomagnetic laboratories and often involve subsampling down to a few milligrams, causing them to be less representative of the sediment.

In this paper, we present a rock magnetic study of sediments from Hydrate Ridge recovered during Leg 204. Our data set is based on several artificially induced magnetic properties that can be produced and measured in most paleomagnetic laboratories and may be used as a diagnostic for the presence of magnetic iron sulfides. We tentatively discuss the data in connection with the presence of gas hydrates within the gas hydrate stability zone (GHSZ) and also with the probable former occurrence of gas hydrates at deeper locations. Detailed identification of the magnetic mineralogy and interpretation of the data, as well as a cross-comparison with hysteresis parameters, will be presented elsewhere. The data set reported here is compiled in Tables T1, T2, T3, T4, T5, T6, T7, T8, and T9, and the most relevant results are plotted in Figures F3, F4, F5, F6, F7, F8, F9, F10, F11, and F12.

## METHODS

About 550 sediment samples were collected using 8-cm<sup>3</sup> plastic boxes during Leg 204. Samples were taken at a resolution of 10 m (1/core), except in selected intervals such as the BSR, Horizons A, B, and B', and in the vicinity of gas hydrates, where sampling resolution was tightened up to 1.5 m (1/section). To minimize sample dehydration and alteration, samples were packed in sealed, nitrogen-filled bags and stored in a cold environment until they were processed in the laboratory.

Rock magnetic properties were measured at the Paleomagnetic Laboratory (CSIC-UB) of the Institute of Earth Sciences “Jaume Almera” in Barcelona, Spain. Rock magnetic measurements include low-field magnetic susceptibility ( $\chi$ ), anhysteretic remanent magnetization (ARM), and isothermal remanent magnetization (IRM). Low-field magnetic susceptibility was measured with a KLY-2 susceptibility bridge using a field of 0.1 mT at a frequency of 470 Hz. ARM was imparted using a home-made experimental set up that consisted of the application of a peak alternating field (AF) of 0.1 T (imparted with a Shonstedt AF demagnetizer without the magnetic shielding) in the same direction as a bias field of 0.05 mT (imparted with a set of Helmholtz coils). Two IRMs, which we refer to as IRM@0.1T and IRM@0.9T, were imparted using a Molspin pulse magnetizer with two fields of 0.1 and 0.9 T, respectively. The ARM, IRM@0.1T, and IRM@0.9T were measured using a 2G Enterprises three-axis cryogenic magnetometer. Because of their very high intensities, the IRM@0.1T and IRM@0.9T could not be measured for some samples. In addition, technical problems prevented a reliable measurement of the ARM in a few samples. All magnetic properties are normalized by the dry weight of the samples.

**T1.** Rock magnetic data, Site 1244, p. 22.

**T2.** Rock magnetic data, Site 1245, p. 23.

**T3.** Rock magnetic data, Site 1246, p. 25.

**T4.** Rock magnetic data, Site 1247, p. 26.

**T5.** Rock magnetic data, Site 1248, p. 27.

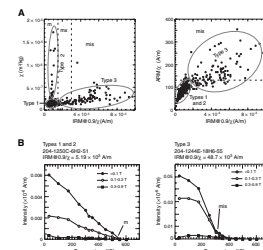
**T6.** Rock magnetic data, Site 1249, p. 28.

**T7.** Rock magnetic data, Site 1250, p. 29.

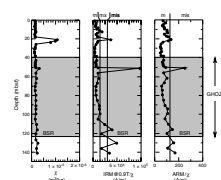
**T8.** Rock magnetic data, Site 1251, p. 30.

**T9.** Rock magnetic data, Site 1252, p. 32.

**F3.** IRM@0.9T/ $\chi$  vs.  $\chi$  and ARM/ $\chi$  data, p. 12.



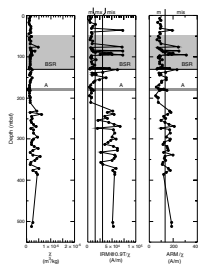
**F4.** Rock magnetic data, Site 1244, p. 13.



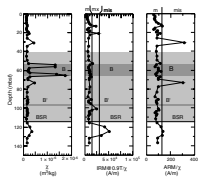
ARM, IRM@0.1T, and IRM@0.9T values are related to the concentration of magnetic minerals, regardless of their type. Magnetic susceptibility has been classically used as a proxy for the concentration of magnetic minerals. However, caution must be exercised when using magnetic susceptibility because it is also influenced by nonmagnetic typical rock-forming minerals such as clays, quartz, and carbonates. In addition to these magnetic properties, we obtained additional rock magnetic parameters by calculating interparametric ratios. Because magnetic iron sulfides have magnetic properties slightly different from those of magnetite, such interparametric ratios can be used to distinguish between these minerals. Among the different parameters calculated, of particular interest is the IRM@0.9T/ $\chi$  ratio. This ratio has been used to infer the presence of greigite (Roberts, 1995; Dekkers et al., 2000) and to discriminate between greigite and pyrrhotite (Housen and Musgrave, 1996) in sediment samples. A recent compilation of rock magnetic data of known magnetic assemblages (Peters and Dekkers, 2003) allows improved interpretation of IRM@0.9T/ $\chi$  ratios in terms of specific magnetic minerals. In the absence of iron hydroxides such as hematite and goethite, magnetite-dominated samples have IRM@0.9T/ $\chi$  ratios that usually range between 1 and 15 kA/m and only exceptionally exceed 30 kA/m. IRM@0.9T/ $\chi$  ratios for both greigite- and pyrrhotite-dominated samples are typically higher than 30 kA/m and very rarely lower than 15 kA/m. Such high IRM@0.9T/ $\chi$  values result from the single-domain (SD) behavior that magnetic iron sulfides show in most natural samples (Roberts, 1995; Dekkers et al., 2000). According to this, IRM@0.9T/ $\chi$  ratios of up to 15 kA/m might be diagnostic for magnetite-dominated assemblages, whereas IRM@0.9T/ $\chi$  ratios larger than 30 kA/m might discriminate magnetic iron sulfide-dominated samples. Intermediate values between 15 and 30 kA/m likely indicate mixtures of variable amounts of magnetite and magnetic iron sulfides. Thermal demagnetization data of a three-component IRM applied at fields of 0.9, 0.3, and 0.1 T along the three orthogonal axes of the samples (Lowie, 1990) was performed on selected samples with variable IRM@0.9T/ $\chi$  values in order to determine the magnetic mineralogy and to support the interpretation based on these data (Fig. F3).

Besides IRM@0.9T/ $\chi$ , other parameters such as IRM@0.1T/IRM@0.9T, IRM@0.9T-IRM@0.1T, and IRM@0.9T/ARM were also calculated. The IRM@0.1T/IRM@0.9T ratio is equivalent to the s-ratio (e.g., Verosub and Roberts, 1995) measured with a backfield of 0.1 T and indicates the relative proportion between low-coercivity (<0.1 T) and high-coercivity (0.1–0.9 T) magnetic minerals. IRM@0.9T-IRM@0.1T values are equivalent to the HIRM (e.g., Verosub and Roberts, 1995) measured with a backfield of 0.1 T and indicate the proportion of high-coercivity (0.1–0.9 T) magnetic minerals. Because magnetic iron sulfides usually have coercivity values larger than those of magnetite (e.g., Horng et al., 1998), IRM@0.1T/IRM@0.9T ratios can provide information about the relative proportion of magnetic iron sulfides, whereas IRM@0.9T-IRM@0.1T values can provide information about their concentration. IRM@0.9T/ARM might be also used for discriminating between magnetic iron sulfides and magnetite because they respond differently to IRM and ARM acquisition experiments. Although IRM@0.1T/IRM@0.9T, IRM@0.9T-IRM@0.1T, and IRM@0.9T/ARM might therefore be used for examining the occurrence of magnetic iron sulfides, they will not be considered at depth in the present report because their use is not straightforward and still needs to be tested against detailed rock magnetic measurements. Finally, ARM/ $\chi$  ratios were also calculated. We

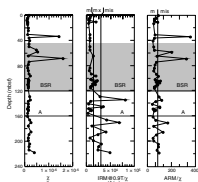
F5. Rock magnetic data, Site 1245, p. 14.



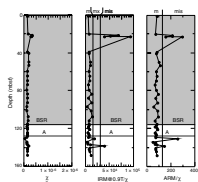
F6. Rock magnetic data, Site 1246, p. 15.



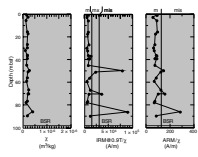
F7. Rock magnetic data, Site 1247, p. 16.



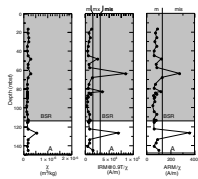
F8. Rock magnetic data, Site 1248, p. 17.



F9. Rock magnetic data, Site 1249, p. 18.



F10. Rock magnetic data, Site 1250, p. 19.



used this ratio to provide hints on the occurrence of magnetic iron sulfides for those samples whose IRMs could not be measured because of their high intensities (see “**Results**,” below).

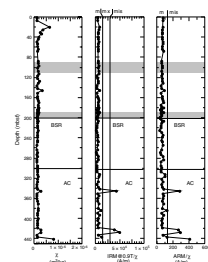
## RESULTS

In Figure F3A, a comparison between  $\text{IRM}@0.9\text{T}/\chi$  and  $\chi$  for all sites is shown. Samples can be divided into three groups. The first group is characterized by low  $\chi$  ( $<3 \times 10^{-7} \text{ m}^3/\text{kg}$ ) and low  $\text{IRM}@0.9\text{T}/\chi$  ( $<1.5 \times 10^{-4} \text{ A/m}$ ) values and is labeled as Type 1. The second group of samples, named Type 2, is characterized by similarly low  $\text{IRM}@0.9\text{T}/\chi$  and higher  $\chi$  (up to  $1.7 \times 10^{-6} \text{ m}^3/\text{kg}$ ) values. The third group, referred to as Type 3, is characterized by high  $\text{IRM}@0.9\text{T}/\chi$  values (between 2 and  $10 \times 10^{-5} \text{ A/m}$ ) and  $\chi$  values slightly larger than those characterizing Type 1 samples (between  $1.5$  and  $6 \times 10^{-7} \text{ m}^3/\text{kg}$ ).

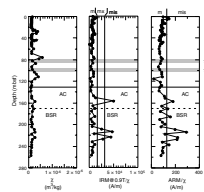
Type 1 samples are the most abundant (70%–75%) and correspond to the hemipelagic and silty clays that predominate in Hydrate Ridge sediments. Type 2 samples are scarce (<2%) and correspond to fine-grained turbidite layers such as those found in Horizon B in Hole 1246B (Fig. F6) and in the debris flow units in Holes 1251B, 1251D (Fig. F11), and 1252A (Fig. F12). According to their  $\text{IRM}@0.9\text{T}/\chi$  values, Type 1 and 2 samples can be interpreted as dominated by magnetite. Increasingly high  $\chi$  values that distinguish Type 2 from Type 1 samples are attributed to an increased proportion of magnetite grains that might have been transported by turbidite currents or in reworked sediments. Noticeably, volcanic ash- and glass-rich intervals, such as those characterizing Horizon A at Sites 1245 and 1248, do not show an enhancement in magnetite, which is the magnetic mineral present according to the low  $\text{IRM}@0.9\text{T}/\chi$  values (Figs. F5, F7, F8). In contrast, these volcanic ash- and glass-rich intervals show a small but significant decrease in the amount of magnetite and can be included within Type 1 samples. The remaining 20%–25% of the studied samples belong to Type 3. These samples correspond to hemipelagic clays and silty clays that, in many cases, contain millimeter- to centimeter-scale iron sulfide nodules. We notice that Type 3 samples do not form a proper cluster but follow a trend between high  $\text{IRM}@0.9\text{T}/\chi$  values, typical for “pure” Type 3 behavior, and low  $\text{IRM}@0.9\text{T}/\chi$  values, typical for Type 1 samples. We interpret this trend as a result of an increased proportion of magnetic iron sulfides in magnetite-dominated hemipelagic clays. Thus,  $\text{IRM}@0.9\text{T}/\chi$  values between  $1.5$  and  $3 \times 10^{-4} \text{ A/m}$  indicate a mixture of magnetite and magnetic iron sulfides, whereas  $\text{IRM}@0.9\text{T}/\chi$  larger than  $3 \times 10^{-4} \text{ A/m}$  indicate magnetic iron sulfide-dominated samples.

Thermal demagnetization data of a three-component IRM (Fig. F3B) validates the interpretation based on  $\text{IRM}@0.9\text{T}/\chi$  results. Type 1 and 2 samples are characterized by a steady decrease in the intensity of the three IRM components, which disappear completely below  $600^\circ\text{C}$ . This indicates the predominance of magnetite and the absence of hematite. Lack of a sharp decrease in IRM intensities below  $175^\circ\text{C}$  also indicates the absence of goethite. Moreover, no significant decrease in IRM intensities is seen below  $350^\circ\text{C}$ , which indicates a negligible contribution of magnetic iron sulfides. Type 3 samples show a rather different IRM demagnetization pattern. IRM intensities show a sharp decrease below  $300^\circ\text{C}$ , which indicates the presence of magnetic iron sulfides such as greigite or pyrrhotite (e.g., Roberts, 1995). Above  $300^\circ\text{C}$ , the remaining IRM intensity is very low and mostly demagnetized by  $450^\circ\text{C}$ , indicat-

F11. Rock magnetic data, Site 1251, p. 20.



F12. Rock magnetic data, Site 1252, p. 21.



ing a rather small contribution of magnetite. The lack of a sharp decay in IRM intensities below 175°C and the complete removal of the IRM below 500°C indicate the absence of goethite and hematite, respectively, and validate the use of  $\text{IRM}@0.9\text{T}/\chi$  ratios for discriminating magnetite- and iron sulfide-dominated assemblages.

We notice that some Type 3 samples, including those containing large magnetic iron sulfide nodules, do not appear in the diagram shown in Figure F3 because IRMs were too intense to be measured (see “**Methods**,” p. 3). In order to allow potential identification of magnetic iron sulfides in these samples, we have compared  $\text{IRM}@0.9\text{T}/\chi$  with  $\text{ARM}/\chi$  values (Fig. F3A). Both parameters show an overall positive correlation that becomes somewhat noisy for high  $\text{IRM}@0.9\text{T}/\chi$  and  $\text{ARM}/\chi$  values. In any case, we notice that only few magnetite-dominated samples (only 6 out of ~400) with  $\text{IRM}@0.9\text{T}/\chi$  values lower than  $1.5 \times 10^{-4}$  A/m, show  $\text{ARM}/\chi$  values higher than 130 A/m. On the contrary, such an  $\text{ARM}/\chi$  value of 130 A/m is surpassed by most magnetic iron sulfide-dominated samples (with  $\text{IRM}@0.9\text{T}/\chi$  values higher than  $1.5 \times 10^{-4}$  A/m). This suggests that, in the absence of IRM data, a threshold  $\text{ARM}/\chi$  value of ~130 A/m can be also used to identify samples with a significant proportion of magnetic iron sulfides.

## DISCUSSION

Depth variations observed for the  $\text{IRM}@0.9\text{T}/\chi$  and  $\text{ARM}/\chi$  ratios at different sites illustrate the spatial distribution of magnetic iron sulfides within Hydrate Ridge sediments (Figs. F4, F5, F6, F7, F8, F9, F10, F11, F12). Overall, high  $\text{IRM}@0.9\text{T}/\chi$  and  $\text{ARM}/\chi$  ratios are very common above the BSR. We notice that  $\text{IRM}@0.9\text{T}/\chi$  and  $\text{ARM}/\chi$  peaks are more common within the gas hydrate occurrence zone (GHOZ) and appear only eventually above it. The peaked pattern of  $\text{IRM}@0.9\text{T}/\chi$  and  $\text{ARM}/\chi$  values suggests that the distribution of magnetic iron sulfides is usually very heterogeneous, and so is the distribution of gas hydrates within the GHOZ, which can vary from <2% to >20% of the pore space within few meters (Tréhu et al., 2003, 2004b). The only two sites where magnetic iron sulfides are absent within the GHSZ are Sites 1251 and 1252, where the lowest concentrations of gas hydrates are found (Tréhu, Bohrmann, Rack, Torres, et al., 2003; Tréhu et al., 2004b). These results seem to confirm previous interpretations linking gas hydrate occurrence and formation of magnetic iron sulfides (Housen and Musgrave, 1996), suggesting that magnetic methods may be also used for assessing the distribution of gas hydrates. Further comparison between magnetic data and detailed estimations of gas hydrate content will be necessary in order to explore in depth the reliability of magnetic methods.

According to the  $\text{IRM}@0.9\text{T}/\chi$  and  $\text{ARM}/\chi$  ratios, magnetic iron sulfides appear to be also very common within the interval located ~30–50 m just below the BSR, which is evident at some sites (e.g., Figs. F5, F6, F7). These magnetic iron sulfide-rich intervals correlate with the location of a secondary BSR reported from MCS data (Bangs et al., 2005). They have been interpreted as “fossil BSRs” that mark the former position of the base of the gas hydrate stability zone before gas hydrates dissociated as a result of changing temperature and pressure conditions since the Last Glacial Maximum (Housen and Musgrave, 1996; Musgrave et al., 2005).

Finally, we notice that at several sites magnetic iron sulfides are present at positions far deeper than the BSR and the fossil BSR, even in sediments from the accretionary wedge (e.g., Figs. F5, F11, F12). Given

the apparent link between magnetic iron sulfides and gas hydrates, we interpret this to mean that the presence of magnetic iron sulfides at these deeper positions suggests the former presence of gas hydrates formed during earlier stages of the evolution of Hydrate Ridge.

## **ACKNOWLEDGMENTS**

This research used samples and/or data provided by the Ocean Drilling Program (ODP). ODP is sponsored by the U.S. National Science Foundation (NSF) and participating countries under the management of Joint Oceanographic Institutions (JOI), Inc. We thank the captain, the crew, technicians, and fellow scientists aboard the *JOIDES Resolution* for their assistance during Leg 204. We also thank the Paleomagnetic Laboratory (Serveis de Suport a la Recerca UB-CSIC) of the Institute of Earth Sciences in Barcelona, where rock magnetic measurements were conducted. B. Housen is thanked for his constructive review. The Spanish Ministry of Science and Education (Ministerio de Educación y Ciencia, MEC) funded participation of E. Gràcia in ODP Leg 204 through grant REN 2001-5262-E and sample analysis and processing through grant BTE2002-11698-E. J.C. Larrasoña benefits from a MEC "Ramon y Cajal" contract and E. Piñero benefits from a MEC Ph.D. fellowship AP2003-2872.

## REFERENCES

- Bangs, N.L.B., Musgrave, R.J., and Tréhu, A.M., 2005. Upward shifts in the southern Hydrate Ridge gas hydrate stability zone following postglacial warming, offshore Oregon. *J. Geophys. Res.*, 110. doi:[10.1029/2004JB003293](https://doi.org/10.1029/2004JB003293)
- Dekkers, M.J., Passier, H.F., and Schoonen, M.A.A., 2000. Magnetic properties of hydrothermally synthesized greigite ( $\text{Fe}_3\text{S}_4$ ). II. High- and low-temperature characteristics. *Geophys. J. Int.*, 141:809–819. doi:[10.1046/j.1365-246x.2000.00129.x](https://doi.org/10.1046/j.1365-246x.2000.00129.x)
- Housen, B.A., and Musgrave, R.J., 1996. Rock-magnetic signature of gas hydrates in accretionary prism sediments. *Earth Planet. Sci. Lett.*, 139:509–519. doi:[10.1016/0012-821X\(95\)00245-8](https://doi.org/10.1016/0012-821X(95)00245-8)
- Horng, C.-S., Torii, M., Shea, K.-S., and Kao S.-J., 1998. Inconsistent magnetic polarities between greigite- and pyrrhotite/magnetite-bearing marine sediments from the Tsailiao-chi section, southwestern Taiwan. *Earth Planet. Sci. Lett.*, 164:467–481. doi:[10.1016/S0012-821X\(98\)00239-8](https://doi.org/10.1016/S0012-821X(98)00239-8)
- Kasten, S., Freudenthal, T., Gingele, F.X., and Schulz, H.D., 1998. Simultaneous formation of iron-rich layers at different redox boundaries in sediments of the Amazon deep-sea fan. *Geochim. Cosmochim. Acta*, 62:2253–2264. doi:[10.1016/S0016-7037\(98\)00093-3](https://doi.org/10.1016/S0016-7037(98)00093-3)
- Lowrie, W., 1990. Identification of ferromagnetic minerals in a rock by coercivity and unblocking temperature properties. *Geophys. Res. Lett.*, 17:159–162.
- Musgrave, R.J., Bangs, N.L., Larrasoña, J.C., Gràcia, E., Hollamby, J.A., and Vega, M.E., 2005. Rise of the base of the gas hydrate zone since the last glacial recorded by rock magnetism. *Geology*, 34:117–120. doi:[10.1130/G22008.1](https://doi.org/10.1130/G22008.1)
- Neretin, L.N., Böttcher, M.E., Jørgensen, B.B., Volkov, I.I., Lüschen, H., and Hilgenfeldt, K., 2004. Pyritization processes and greigite formation in the advancing sulphidation front in the upper Pleistocene sediments of the Black Sea. *Geochim. Cosmochim. Acta*, 68:2081–2093. doi:[10.1016/S0016-7037\(03\)00450-2](https://doi.org/10.1016/S0016-7037(03)00450-2)
- Peters, C., and Dekkers, M., 2003. Selected room-temperature magnetic parameters as a function of mineralogy, concentration and grain size. *Phys. Chem. Earth*, 28:659–667. doi:[10.1016/S1474-7065\(03\)00120-7](https://doi.org/10.1016/S1474-7065(03)00120-7)
- Roberts, A.P., 1995. Magnetic properties of sedimentary greigite ( $\text{Fe}_3\text{S}_4$ ). *Earth Planet. Sci. Lett.*, 134:227–236. doi:[10.1016/0012-821X\(95\)00131-U](https://doi.org/10.1016/0012-821X(95)00131-U)
- Roberts, A.P., and Weaver, R., 2005. Multiple mechanisms of remagnetization involving sedimentary greigite ( $\text{Fe}_3\text{S}_4$ ). *Earth Planet. Sci. Lett.*, 231:263–277. doi:[10.1016/j.epsl.2004.11.024](https://doi.org/10.1016/j.epsl.2004.11.024)
- Shipboard Scientific Party, 2003. Leg 204 summary. In Tréhu, A.M., Bohrmann, G., Rack, F.R., Torres, M.E., et al., *Proc. ODP, Init. Repts.*, 204: College Station TX (Ocean Drilling Program), 1–75. [HTML]
- Tréhu, A.M., Bangs, N.L., Arsenault, M.A., Bohrmann, G., Goldfinger, C., Johnson, J.E., Nakamura, Y., and Torres, M.E., 2002. Complex subsurface plumbing beneath southern Hydrate Ridge, Oregon continental margin, from high-resolution 3-D seismic reflection and OBS data. *Fourth Int. Conf. Gas Hydrates*, 19023:90–96.
- Tréhu, A.M., Bohrmann, G., Rack, F.R., Torres, M.E., et al., 2003. *Proc. ODP, Init. Repts.*, 204 [CD-ROM]. Available from: Ocean Drilling Program, Texas A&M University, College Station TX 77845-9547, USA. [HTML]
- Tréhu, A.M., Flemings, P.B., Bangs, N.L., Chevallier, J., Gràcia, E., Johnson, J.E., Liu, C.S., Liu, X., Riedel, M., and Torres, M., 2004a. Feeding methane vents and gas hydrate deposits at south Hydrate Ridge. *Geophys. Res. Lett.*, 31:L23310. doi:[10.1029/2004GL021286](https://doi.org/10.1029/2004GL021286)
- Tréhu, A.M., Long, P.E., Torres, M.E., Bohrmann, G., Rack, F.R., Collett, T.S., Goldberg, D.S., Milkov, A.V., Riedel, M., Schultheiss, P., Bangs, N.L., Barr, S.R., Borowski, W.S., Claypool, G.E., Delwiche, M.E., Dickens, G.R., Gracia, E., Guerin, G., Holland, M., Johnson, J.E., Lee, Y.-J., Liu, C.-S., Su, X., Teichert, B., Tomaru, H., Vanneste, M., Watanabe, M., and Weinberger, J.L., 2004b. Three-dimensional distribution of gas

- hydrate beneath southern Hydrate Ridge: constraints from ODP Leg 204. *Earth Planet. Sci. Lett.*, 222:845–862. [doi:10.1016/j.epsl.2004.03.035](https://doi.org/10.1016/j.epsl.2004.03.035)
- Tréhu, A.M., Torres, M.E., Moore, G.F., Suess, E., and Bohrmann, G., 1999. Temporal and spatial evolution of a gas-hydrate-bearing accretionary ridge on the Oregon continental margin. *Geology*, 27(10):939–942. [doi:10.1130/0091-7613\(1999\)027<0939:TASEOA>2.3.CO;2](https://doi.org/10.1130/0091-7613(1999)027<0939:TASEOA>2.3.CO;2)
- Verosub, K.L., and Roberts, A.P., 1995. Environmental magnetism: past, present, and future. *J. Geophys. Res.*, 100:2175–2192. [doi:10.1029/94JB02713](https://doi.org/10.1029/94JB02713)

**Figure F1.** A. Plate tectonic setting of the Cascadia accretionary margin. Black outlined box shows location of Hydrate Ridge. B. Detailed bathymetric map (20-m contour) showing the location of the ODP Leg 204 drill sites in southern Hydrate Ridge. Red lines indicate the location of the line-drawings shown in Figure F2, p. 11.

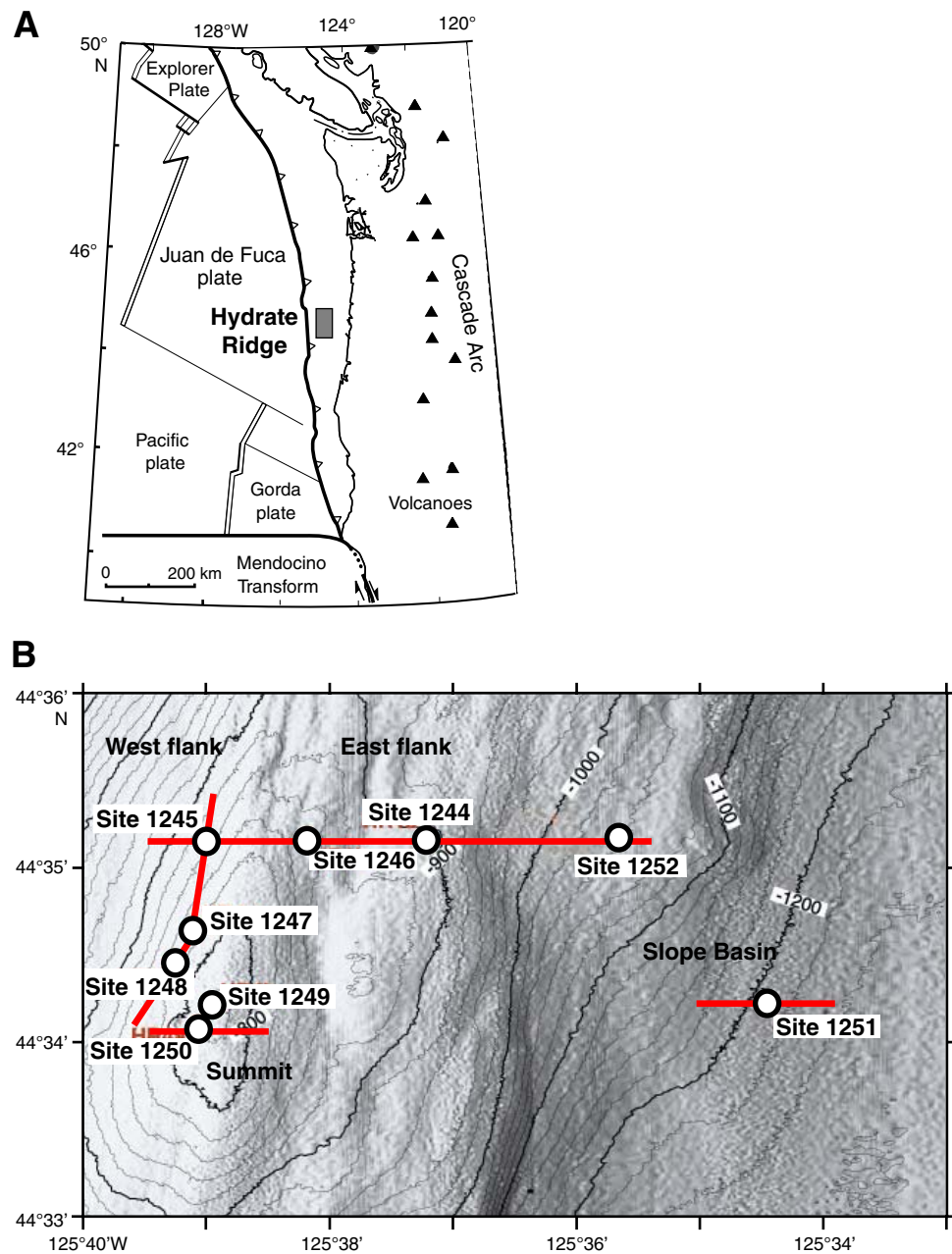


**Figure F2.** Line drawings across different sections of southern Hydrate Ridge, based on 3-D seismic profiles (Tréhu et al., 2004b). A. West–east section across the northern part of southern Hydrate Ridge. B. West–east section across the lowermost part of the slope basin of Hydrate Ridge. C. West–east section across the summit of southern Hydrate Ridge. D. North–south section along the west flank of southern Hydrate Ridge. The bottom-simulating reflector (BSR), main seismic horizons, and Leg 204 drill sites are identified. Data correspond to stratigraphic intervals marked by a thick black line. DF1, DF2 = debris flow units. U = unconformity.

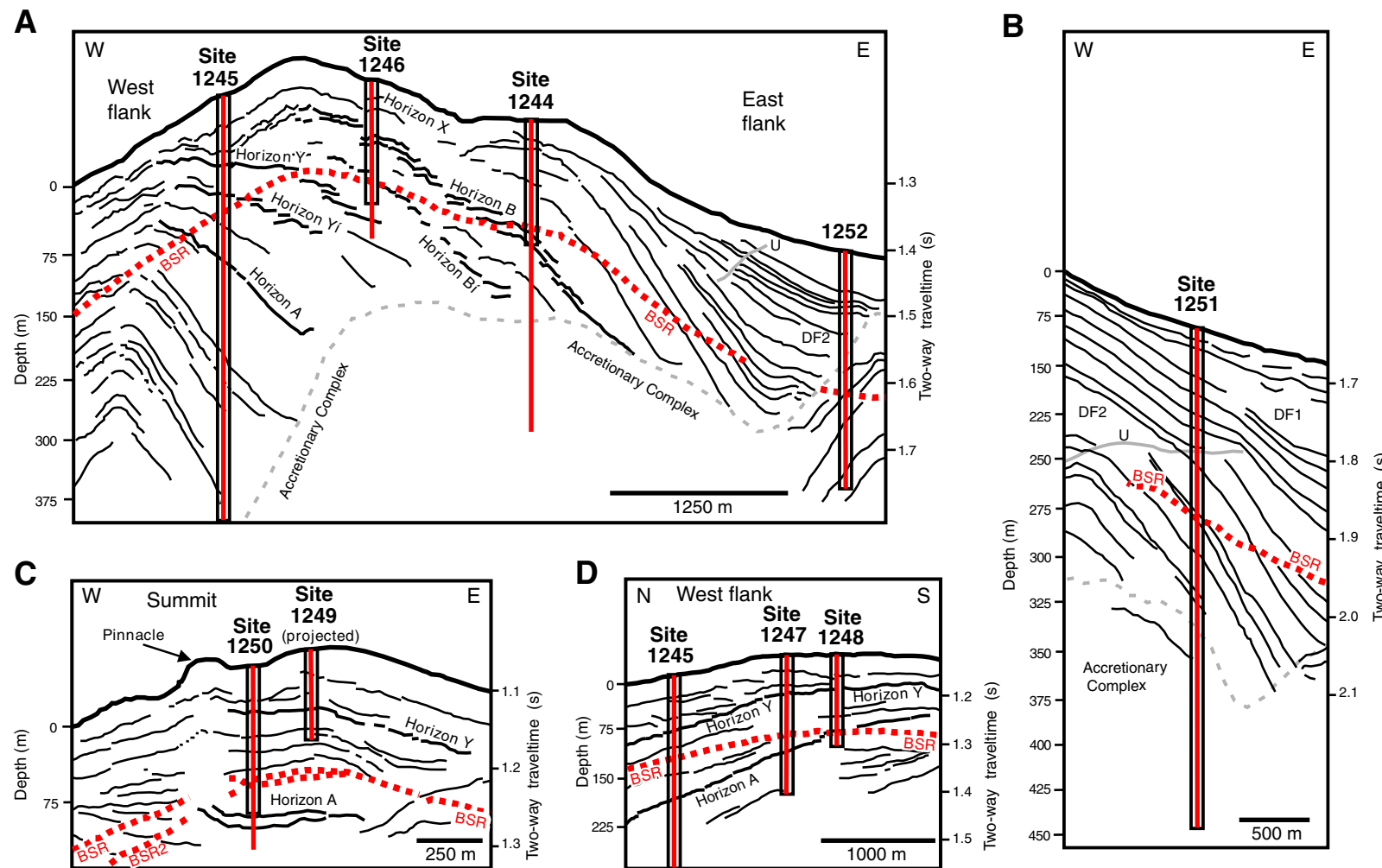


**Figure F3.** A. Comparison of IRM@0.9T/ $\chi$  with  $\chi$  and ARM/ $\chi$  data for all the studied samples. On the left plot, dashed lines mark the fields of m (magnetite-), mis (magnetic iron sulfide-), and mx (mixed-dominated) samples as derived from IRM@0.9T/ $\chi$  ratios. On the right plot, the dashed line separates the field of mis samples as derived from ARM/ $\chi$  values. B. Thermal demagnetization results of representative magnetite-dominated (Types 1 and 2) and magnetic iron sulfide-dominated (Type 3) samples. The presence of magnetite and magnetic iron sulfides is deduced from the sharp decay in IRM intensities below 550° and 300°C, respectively. Note the intensity of the samples, which is one order of magnitude larger for Type 3 samples.

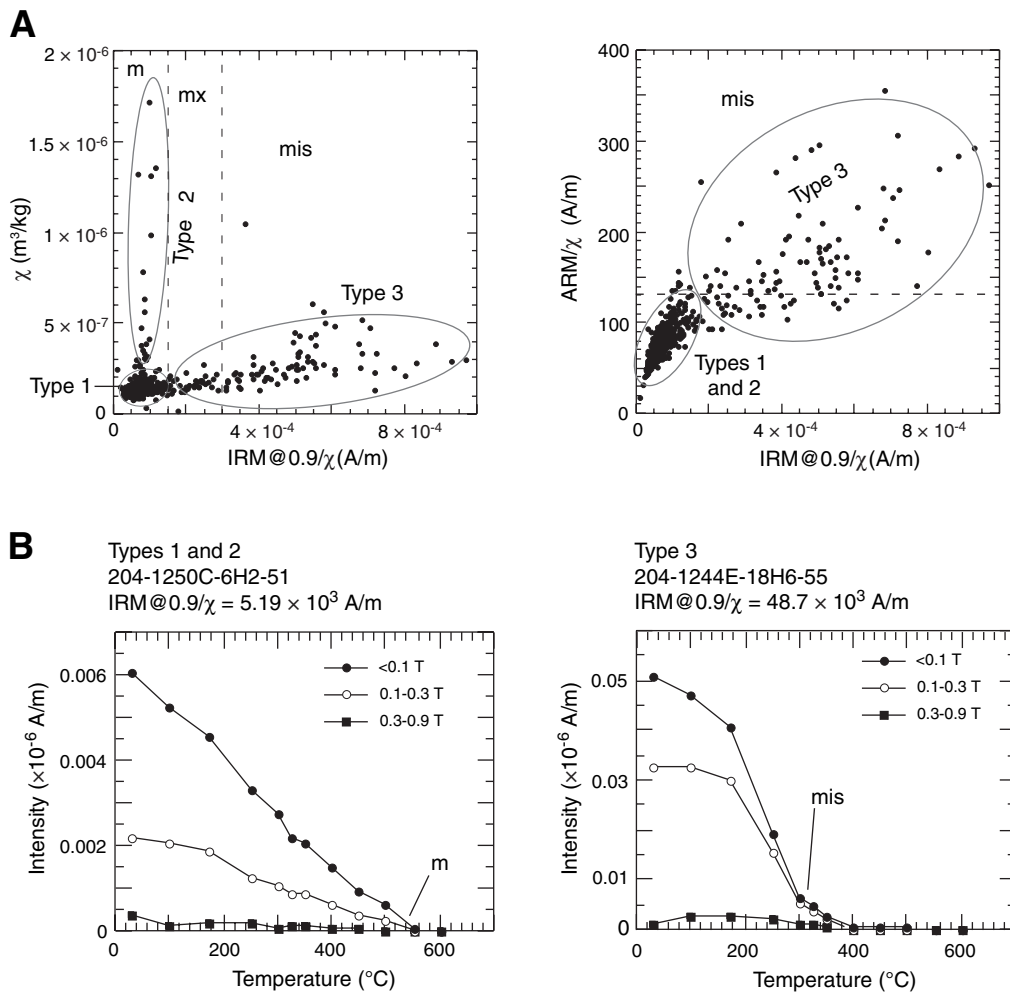


**Figure F4.** Depth variations of selected rock magnetic data ( $\chi$ , IRM@0.9T/ $\chi$ , and ARM/ $\chi$ ) at Site 1244. The position of the bottom-simulating reflector (BSR) is indicated by a dark line, and the gas hydrate occurrence zone (GHOZ) is marked by light gray shading. M, mis, and mx denote magnetite-, magnetic iron sulfide-, and mixed-dominated magnetic assemblages, derived from IRM@0.9T/ $\chi$  and ARM/ $\chi$  data.

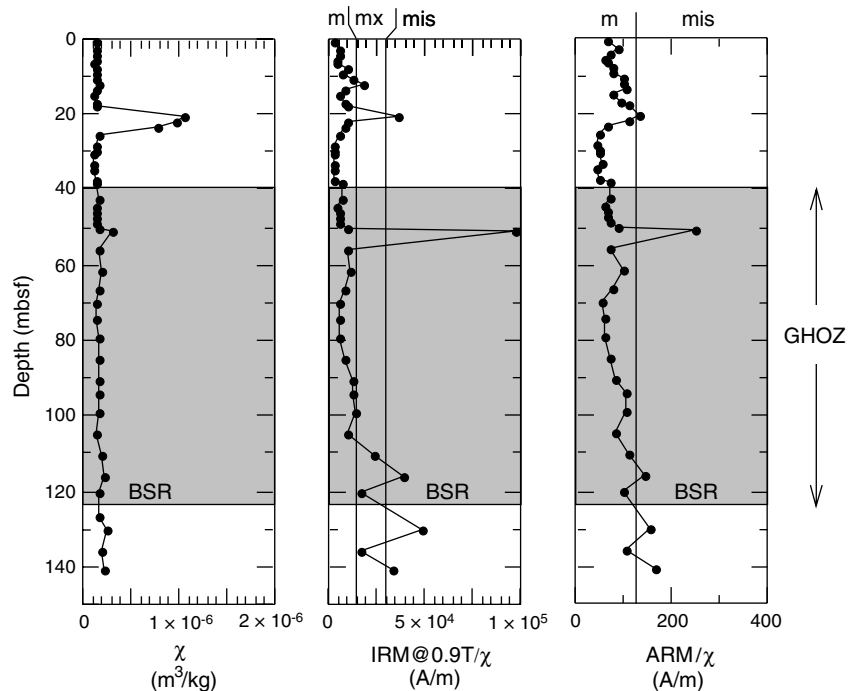


**Figure F5.** Depth variations of selected rock magnetic data ( $\chi$ , IRM@0.9T/ $\chi$ , and ARM/ $\chi$ ) at Site 1245. The position of the bottom-simulating reflector (BSR) is indicated by a dark line, the gas hydrate occurrence zone (GHOZ) is marked by light gray shading, and the position of Horizon A is marked by dark gray shading. M, mis, and mx denote magnetite-, magnetic iron sulfide-, and mixed-dominated magnetic assemblages, respectively, derived from IRM@0.9T/ $\chi$  and ARM/ $\chi$  data.

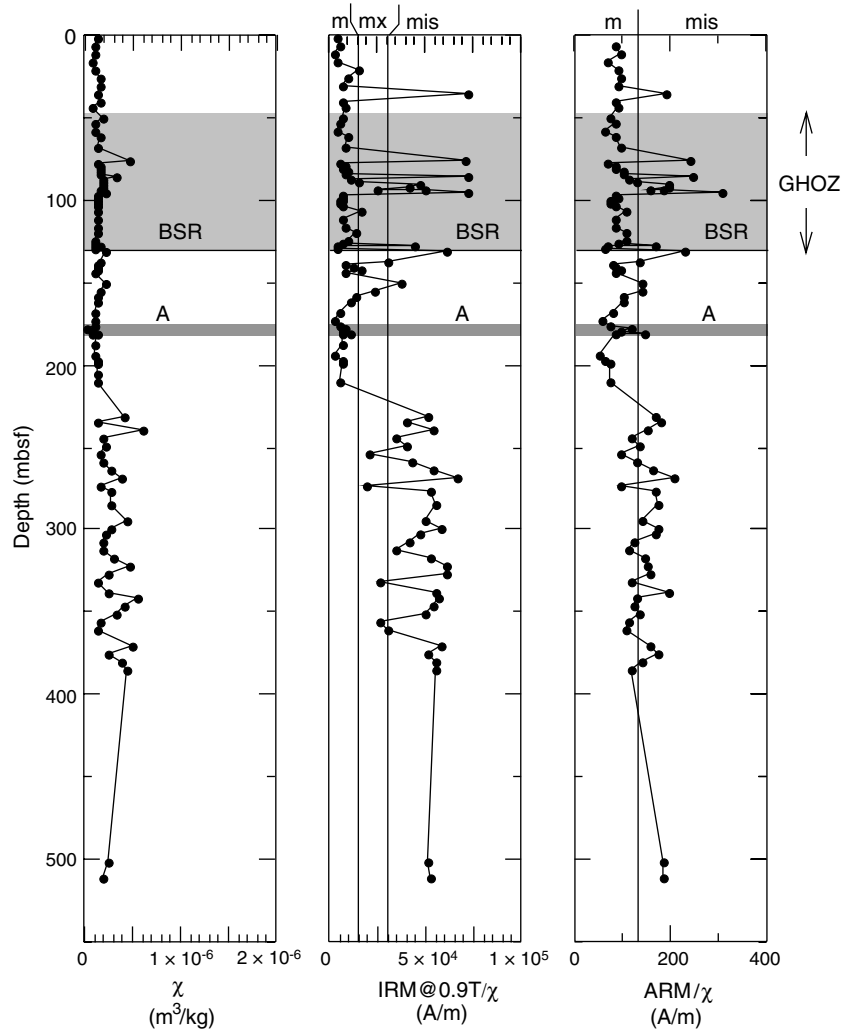


**Figure F6.** Depth variations of selected rock magnetic data ( $\chi$ , IRM@0.9T/ $\chi$ , and ARM/ $\chi$ ) at Site 1246. The position of the bottom-simulating reflector (BSR) is indicated by a dark line, the gas hydrate occurrence zone (GHOZ) is marked by light gray shading, and the positions of Horizons B and B' are marked by dark gray shading. M, mis, and mx denote magnetite-, magnetic iron sulfide-, and mixed-dominated magnetic assemblages, derived from IRM@0.9T/ $\chi$  and ARM/ $\chi$  data.

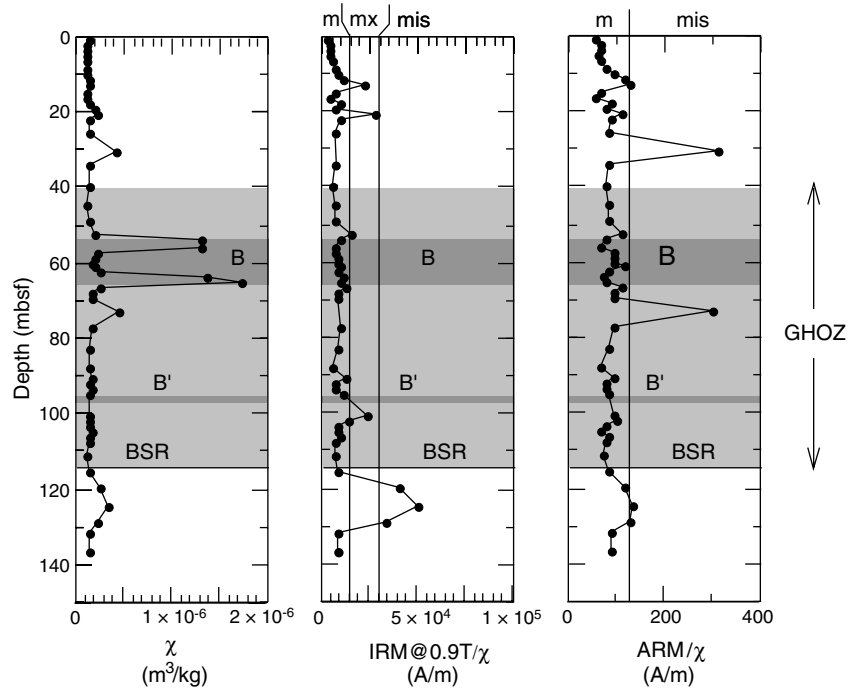


**Figure F7.** Depth variations of selected rock magnetic data ( $\chi$ , IRM@0.9T/ $\chi$ , and ARM/ $\chi$ ) at Site 1247. The position of the bottom-simulating reflector (BSR) is indicated by a dark line, and the gas hydrate occurrence zone (GHOZ) is marked by light gray shading. M, mis, and mx denote magnetite-, magnetic iron sulfide-, and mixed-dominated magnetic assemblages, derived from IRM@0.9T/ $\chi$  and ARM/ $\chi$  data.

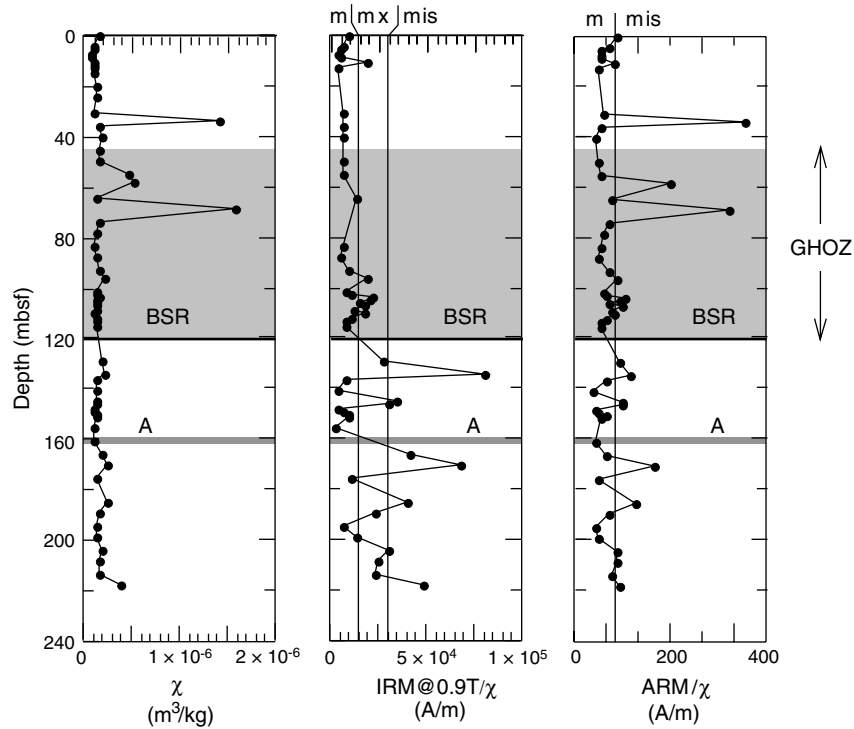


**Figure F8.** Depth variations of selected rock magnetic data ( $\chi$ , IRM@0.9T/ $\chi$ , and ARM/ $\chi$ ) at Site 1248. The position of the bottom-simulating reflector (BSR) is indicated by a dark line, the gas hydrate occurrence zone (GHOZ) is marked by light gray shading, and the position of Horizon A is marked by dark gray shading. M, mis, and mx denote magnetite-, magnetic iron sulfide-, and mixed-dominated magnetic assemblages, respectively, derived from IRM@0.9T/ $\chi$  and ARM/ $\chi$  data.

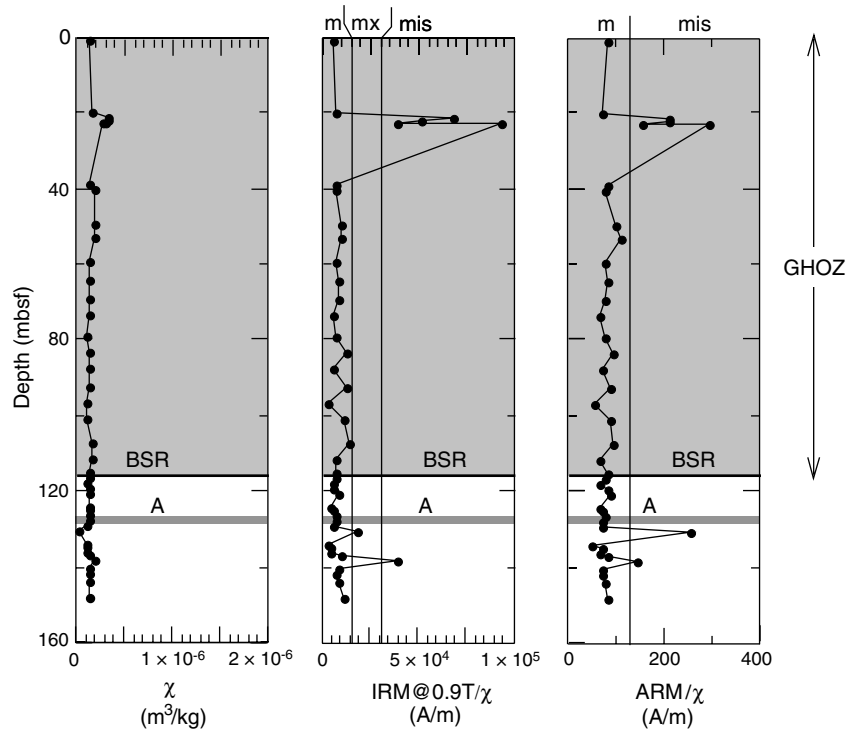


**Figure F9.** Depth variations of selected rock magnetic data ( $\chi$ , IRM@0.9T/ $\chi$ , and ARM/ $\chi$ ) at Site 1249. The position of the bottom-simulating reflector (BSR) is indicated by a dark line, and the gas hydrate occurrence zone (GHOZ) is marked by light gray shading. M, mis, and mx denote magnetite-, magnetic iron sulfide-, and mixed-dominated magnetic assemblages, derived from IRM@0.9T/ $\chi$  and ARM/ $\chi$  data.

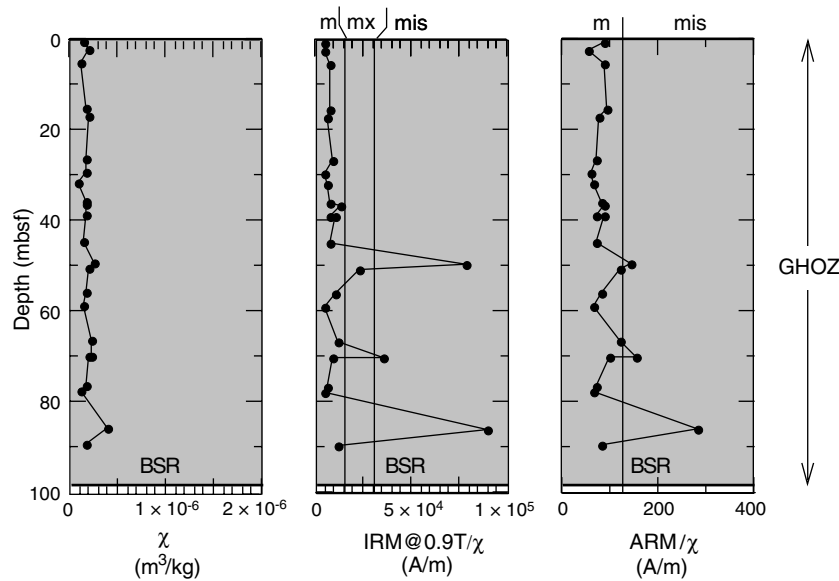


**Figure F10.** Depth variations of selected rock magnetic data ( $\chi$ , IRM@0.9T/ $\chi$ , and ARM/ $\chi$ ) at Site 1250. The position of the bottom-simulating reflector (BSR) is indicated by a dark line, the gas hydrate occurrence zone (GHOZ) is marked by light gray shading, and the position of Horizon A is marked by dark-gray shading. M, mis, and mx denote magnetite-, magnetic iron sulfide-, and mixed-dominated magnetic assemblages, respectively, derived from IRM@0.9T/ $\chi$  and ARM/ $\chi$  data.

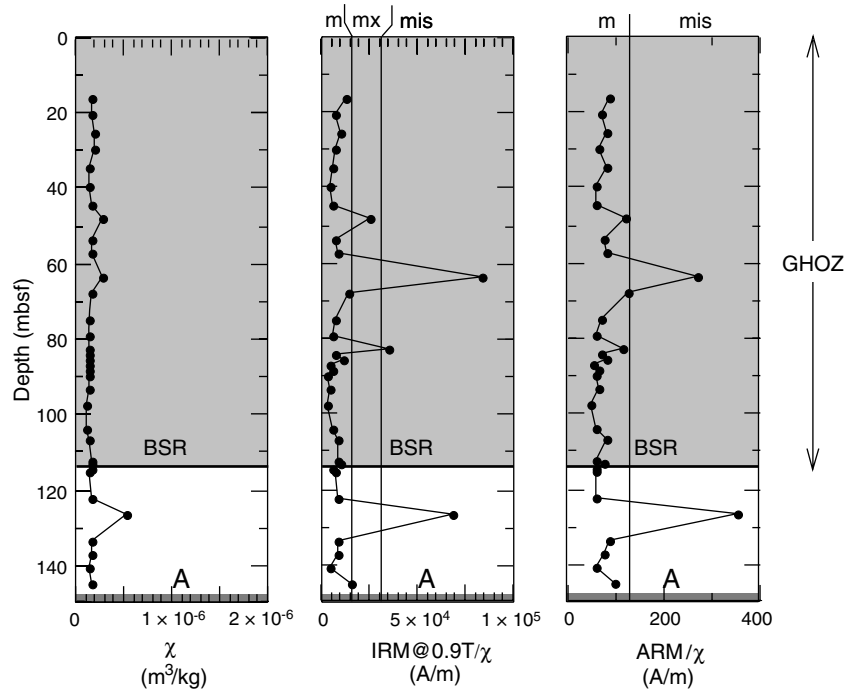


**Figure F11.** Depth variations of selected rock magnetic data ( $\chi$ , IRM@0.9T/ $\chi$ , and ARM/ $\chi$ ) at Site 1251. The position of the bottom-simulating reflector (BSR) is indicated by a dark line, and the gas hydrate occurrence zone (GHOZ) is marked by light gray shading. Stippled area indicates the position of the debris flow unit DF1. AC indicates the top of the accretionary complex. M, mis, and mx denote magnetite-, magnetic iron sulfide-, and mixed-dominated magnetic assemblages, respectively, derived from IRM@0.9T/ $\chi$  and ARM/ $\chi$  data.

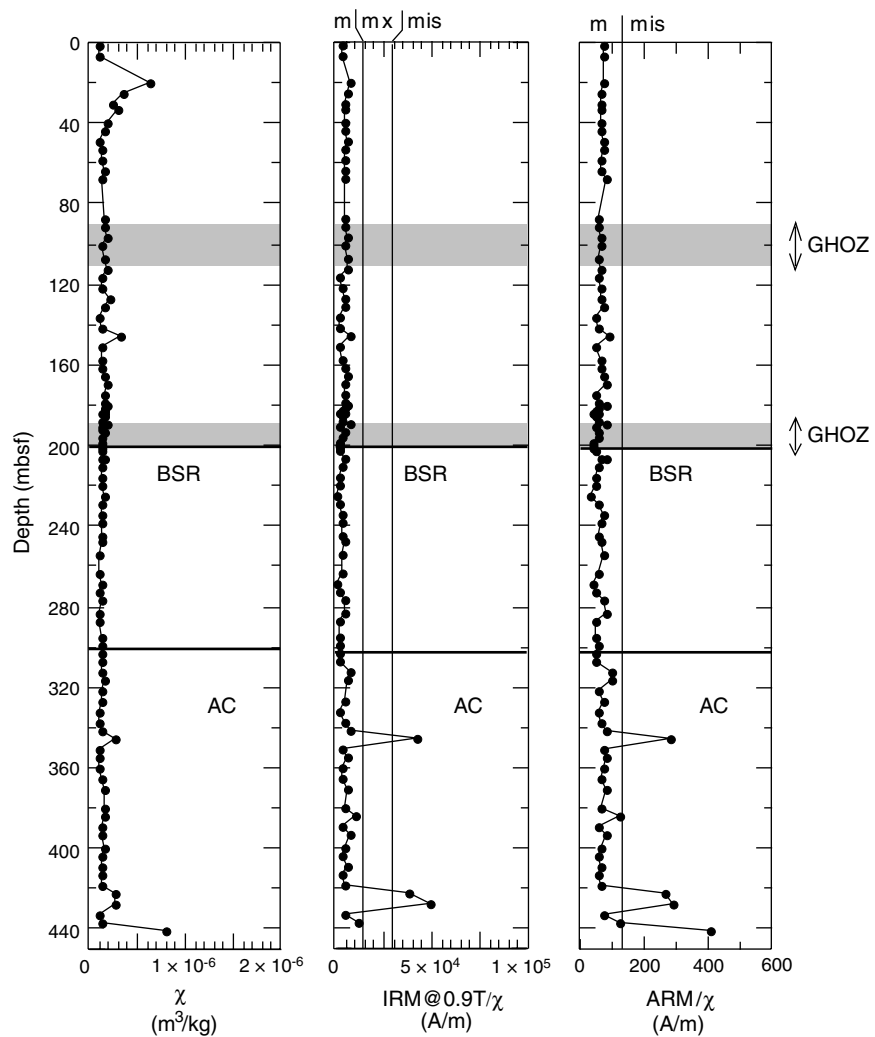


**Figure F12.** Depth variations of selected rock magnetic data ( $\chi$ , IRM@0.9T/ $\chi$ , and ARM/ $\chi$ ) at Site 1252. The estimated position of the bottom-simulating reflector (BSR) is indicated by a dashed dark line (see Tréhu, Bohrmann, Rack, Torres, et al., 2003), and the gas hydrate occurrence zone (GHOZ) is marked by light gray shading. Stippled area = position of the debris flow Unit DF2. AC = the top of the accretionary complex. M, mis, and mx denote magnetite-, magnetic iron sulfide-, and mixed-dominated magnetic assemblages, respectively, derived from IRM@0.9T/ $\chi$  and ARM/ $\chi$  data.

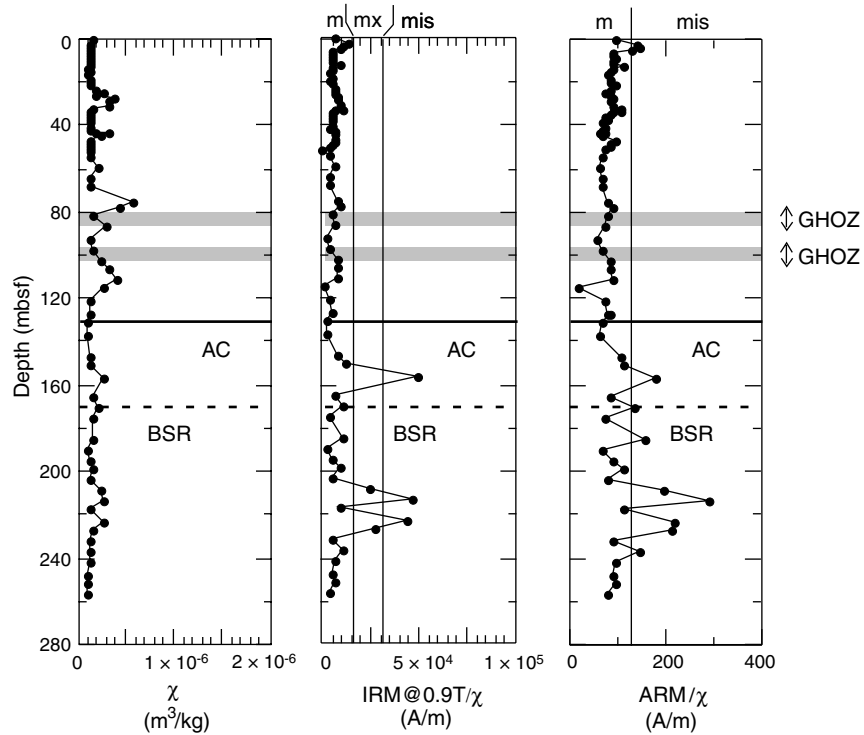


**Table T1.** Rock magnetic data, Site 1244.

Core, section, interval (cm)	Depth (mbsf)	$\chi$ ( $10^{-8}$ m <sup>3</sup> /kg)	ARM ( $10^{-6}$ Am <sup>2</sup> /kg)	IRM@0.1T ( $10^{-4}$ Am <sup>2</sup> /kg)	IRM@0.9T ( $10^{-4}$ Am <sup>2</sup> /kg)	IRM@0.9T/ ARM	IRM@0.1T/ IRM@0.9T	IRM@0.9T- IRM@0.1T ( $10^{-4}$ Am <sup>2</sup> /kg)	IRM@0.9T/ $\chi$ ( $10^3$ A/m)	ARM/ $\chi$ ( $10^3$ A/m)
204-1244E-										
1H-1, 88–90	0.89	14.26	9.19	2.86	4.41	47.99	0.65	1.55	3.09	0.064
1H-2, 106–108	2.57	13.63	12.50	5.06	8.57	68.56	0.59	3.51	6.29	0.092
1H-3, 111–113	4.12	12.77	9.46	3.90	6.42	67.86	0.61	2.52	5.03	0.074
1H-4, 100–102	5.51	13.11	8.02	3.14	5.25	65.46	0.60	2.11	4.00	0.061
1H-5, 38–40	6.39	12.37	8.53	3.32	5.47	64.13	0.61	2.15	4.42	0.069
1H-6, 56–58	8.07	14.48	11.50	8.15	14.90	129.57	0.55	6.75	10.29	0.079
2H-1, 50–52	9.21	13.17	9.91	5.53	9.52	96.06	0.58	3.99	7.23	0.075
2H-2, 50–52	10.71	12.90	12.90	9.39	17.00	131.78	0.55	7.61	13.18	0.100
2H-3, 50–52	12.21	15.84	16.20	15.10	28.80	177.78	0.52	13.70	18.18	0.102
2H-4, 50–52	13.71	14.29	15.30	7.20	12.20	79.74	0.59	5.00	8.54	0.107
2H-5, 50–52	15.21	12.15	9.23	3.88	6.03	65.33	0.64	2.15	4.96	0.076
2H-6, 50–52	16.71	13.85	12.80	7.11	11.20	87.50	0.63	4.09	8.08	0.092
2H-7, 20–22	17.91	15.40	16.90	9.07	14.70	86.98	0.62	5.63	9.55	0.110
4H-1, 50–52	20.71	105.36	143.00	247.00	380.00	265.73	0.65	133.00	36.07	0.136
4H-2, 50–52	22.21	98.67	109.83	80.80	102.00	92.87	0.79	21.20	10.34	0.111
4H-3, 50–52	23.71	78.52	50.50	48.70	61.80	122.38	0.79	13.10	7.87	0.064
4H-4, 50–52	25.21	17.35	8.95	6.69	9.88	110.39	0.68	3.19	5.70	0.052
4H-6, 50–52	28.21	12.90	5.92	2.69	4.25	71.79	0.63	1.56	3.30	0.046
4H-7, 20–22	29.41	12.94	6.35	2.82	4.53	71.32	0.62	1.71	3.50	0.049
5H-1, 50–52	30.21	12.05	6.22	2.41	3.78	60.77	0.64	1.37	3.14	0.052
5H-3, 50–52	33.16	12.37	6.78	2.66	4.14	61.06	0.64	1.48	3.35	0.055
5H-4, 50–52	34.66	11.87	5.57	2.01	3.14	56.37	0.64	1.13	2.65	0.047
5H-6, 50–52	37.66	12.73	6.73	2.85	4.41	65.53	0.65	1.56	3.46	0.053
5H-7, 20–22	38.53	14.19	10.30	6.14	9.25	89.81	0.66	3.11	6.52	0.073
7H-1, 132–134	42.53	16.08	11.40	7.30	11.10	97.37	0.66	3.80	6.90	0.071
7H-3, 52–54	44.71	15.20	9.49	5.03	7.29	76.82	0.69	2.26	4.80	0.062
7H-4, 42–44	46.13	15.29	9.88	6.05	9.14	92.51	0.66	3.09	5.98	0.065
7H-5, 32–34	47.53	14.58	9.50	5.18	8.07	84.95	0.64	2.89	5.53	0.065
7H-6, 23–25	48.94	14.78	11.00	6.12	9.12	82.91	0.67	3.00	6.17	0.074
7H-7, 4–6	50.16	16.01	14.10	10.50	16.50	117.02	0.64	6.00	10.31	0.088
7H-CC, 36–38	50.83	30.37	76.60	194.00	294.00	383.81	0.66	100.00	96.81	0.252
9H-3, 63–65	56.25	16.19	12.00	8.71	15.10	125.83	0.58	6.39	9.32	0.074
9H-7, 54–56	61.71	19.52	19.50	12.50	20.40	104.62	0.61	7.90	10.45	0.100
10H-3, 109–111	66.2	17.06	13.70	9.30	14.90	108.76	0.62	5.60	8.73	0.080
10H-6, 22–24	69.82	14.04	7.83	4.59	7.07	90.29	0.65	2.48	5.04	0.056
12H-1, 43–45	74.04	14.73	8.78	5.63	8.25	93.96	0.68	2.62	5.60	0.060
12H-5, 23–25	78.94	15.77	10.00	6.58	9.60	96.00	0.69	3.02	6.09	0.063
13H-2, 65–67	85.26	16.77	12.20	9.25	13.60	111.48	0.68	4.35	8.11	0.073
13H-6, 102–104	90.93	15.77	13.30	11.80	19.30	145.11	0.61	7.50	12.24	0.084
14H-2, 48–50	94.11	16.54	17.20	14.00	21.20	123.26	0.66	7.20	12.82	0.104
14H-5, 66–68	98.79	17.72	18.80	15.40	24.10	128.19	0.64	8.70	13.60	0.106
16H-1, 42–44	104.53	15.23	12.70	9.19	15.30	120.47	0.60	6.11	10.05	0.083
16H-5, 50–52	110.52	18.65	20.90	27.10	45.00	215.31	0.60	17.90	24.12	0.112
17H-2, 89–91	116	22.43	32.70	46.70	88.20	269.72	0.53	41.50	39.32	0.146
17H-5, 52–54	120.13	18.18	18.70	17.30	29.60	158.29	0.58	12.30	16.28	0.103
18H-3, 57–59	126.68	16.86	0.00	0.00	0.00			0.00	0.00	0.000
18H-6, 54–56	130.4	26.09	40.40	70.00	127.00	314.36	0.55	57.00	48.68	0.155
19H-3, 87–89	136.08	19.62	21.00	20.70	34.00	161.90	0.61	13.30	17.33	0.107
19H-6, 83–85	140.54	23.10	38.50	46.90	77.70	201.82	0.60	30.80	33.63	0.167

Table T2. Rock magnetic data, Site 1245. (Continued on next page.)

Core, section, interval (cm)	Depth (mbsf)	$\chi$ ( $10^{-8} \text{ m}^3/\text{kg}$ )	ARM ( $10^{-6} \text{ Am}^2/\text{kg}$ )	IRM@0.1T ( $10^{-4} \text{ Am}^2/\text{kg}$ )	IRM@0.9T ( $10^{-4} \text{ Am}^2/\text{kg}$ )	IRM@0.9T/ ARM	IRM@0.1T/ IRM@0.9T	IRM@0.9T- IRM@0.1T ( $10^{-4} \text{ Am}^2/\text{kg}$ )	IRM@0.9T/ $\chi$ ( $10^3 \text{ A/m}$ )	ARM/ $\chi$ ( $10^3 \text{ A/m}$ )
204-1245B-										
1H-2, 50-52	2.01	13.69	0.00	4.04	6.18		0.65	2.14	4.51	0.000
1H-5, 50-52	6.51	11.76	9.95	4.25	6.61	66.43	0.64	2.36	5.62	0.085
2H-2, 50-52	11.51	11.28	10.50	2.47	3.67	34.95	0.67	1.20	3.25	0.093
2H-5, 54-56	16.05	9.56	6.30	2.18	3.46	54.92	0.63	1.28	3.62	0.066
3H-2, 50-52	21.01	11.75	10.70	9.80	18.60	173.83	0.53	8.80	15.83	0.091
3H-5, 50-52	25.51	16.28	15.30	11.40	16.50	107.84	0.69	5.10	10.14	0.094
4H-2, 50-52	30.51	17.61	15.50	8.24	12.10	78.06	0.68	3.86	6.87	0.088
4H-5, 50-52	35.01	13.43	25.50	52.20	96.40	378.04	0.54	44.20	71.77	0.190
5H-2, 50-52	40.01	16.84	14.30	7.26	10.70	74.83	0.68	3.44	6.36	0.085
5H-5, 50-52	44.51	9.12	8.02	4.60	7.19	89.65	0.64	2.59	7.88	0.088
6H-2, 50-52	49.51	18.99	13.80	9.18	12.90	93.48	0.71	3.72	6.79	0.073
6H-5, 52-54	54.03	10.99	9.21	4.07	6.44	69.92	0.63	2.37	5.86	0.084
7H-2, 50-52	58.06	11.41	7.30	3.35	5.15	70.55	0.65	1.80	4.51	0.064
7H-5, 52-54	62.11	15.83	13.40	10.30	14.80	110.45	0.70	4.50	9.35	0.085
8H-2, 50-52	68.51	13.96	13.50	8.31	12.50	92.59	0.66	4.19	8.95	0.097
9H-1, 50-52	76.51	47.43	113.00	219.00	334.62	296.12	0.65	115.62	70.55	0.238
9H-2, 50-52	77.83	14.09	9.52	5.32	7.69	80.78	0.69	2.37	5.46	0.068
9H-3, 50-52	79.27	15.92	13.30	8.10	12.30	92.48	0.66	4.20	7.73	0.084
9H-4, 50-52	80.73	16.31	13.60	8.20	12.00	88.24	0.68	3.80	7.36	0.083
9H-5, 50-52	82.23	16.47	16.90	11.30	17.00	100.59	0.66	5.70	10.32	0.103
9H-6, 50-52	83.73	17.33	17.00	9.72	14.90	87.65	0.65	5.18	8.60	0.098
10H-1, 48-50	85.99	33.84	83.20	105.00	244.00	293.27	0.43	139.00	72.10	0.246
10H-2, 47-49	87.47	20.61	22.50	14.30	22.50	100.00	0.64	8.20	10.92	0.109
10H-3, 50-52	88.64	19.24	25.10	19.30	28.50	113.55	0.68	9.20	14.81	0.130
10H-4, 50-52	90.14	20.74	40.10	66.10	98.10	244.64	0.67	32.00	47.30	0.193
10H-5, 50-52	91.64	20.01	39.10	50.40	83.80	214.32	0.60	33.40	41.87	0.195
10H-6, 53-55	93.17	17.90	28.00	29.70	43.60	155.71	0.68	13.90	24.36	0.156
10H-7, 05-07	94.01	18.39	33.90	51.20	92.00	271.39	0.56	40.80	50.03	0.184
11H-1, 55-57	95.56	22.63	69.30	75.30	162.00	233.77	0.46	86.70	71.59	0.306
11H-2, 50-52	96.48	14.09	11.80	6.49	9.78	82.88	0.66	3.29	6.94	0.084
11H-3, 49-51	97.97	13.92	12.40	6.78	10.40	83.87	0.65	3.62	7.47	0.089
11H-4, 88-90	99.87	14.00	10.70	6.04	9.18	85.79	0.66	3.14	6.56	0.076
11H-5, 50-52	100.98	13.60	9.85	8.24	8.50	86.29	0.97	0.26	6.25	0.072
11H-6, 58-60	102.56	13.46	9.58	5.22	8.01	83.61	0.65	2.79	5.95	0.071
11H-7, 50-52	103.98	13.83	11.70	7.01	10.30	88.03	0.68	3.29	7.45	0.085
12H-2, 50-52	106.48	13.51	14.20	15.00	22.20	156.34	0.68	7.20	16.44	0.105
12H-5, 50-52	110.98	13.54	11.10	6.49	10.20	91.89	0.64	3.71	7.53	0.082
13H-2, 53-55	116.01	12.99	10.90	6.67	10.20	93.58	0.65	3.53	7.85	0.084
13H-5, 53-55	120.27	13.80	14.40	12.80	19.20	133.33	0.67	6.40	13.92	0.104
14H-2, 50-52	124.61	11.80	12.50	7.13	10.90	87.20	0.65	3.77	9.23	0.106
14H-3, 38-40	125.99	12.56	10.90	6.21	9.53	87.43	0.65	3.32	7.59	0.087
14H-4, 40-42	127.37	17.01	28.40	42.20	76.40	269.01	0.55	34.20	44.91	0.167
15X-1, 50-52	128.31	12.00	7.77	3.62	5.52	71.04	0.66	1.90	4.60	0.065
15X-3, 50-52	129.87	11.89	7.57	3.20	4.74	62.62	0.68	1.54	3.99	0.064
15X-4, 50-52	131.37	22.48	51.00	74.90	137.00	268.63	0.55	62.10	60.94	0.227
16X-1, 49-52	138.01	17.70	24.10	29.50	55.00	228.22	0.54	25.50	31.07	0.136
16X-2, 50-52	139.57	14.41	10.90	7.11	11.60	106.42	0.61	4.49	8.05	0.076
16X-3, 50-52	141.01	13.59	11.70	9.17	16.50	141.03	0.56	7.33	12.14	0.086
16X-4, 50-52	142.51	13.01	12.50	11.70	21.40	171.20	0.55	9.70	16.45	0.096
16X-5, 50-52	144.01	11.78	9.76	6.13	9.77	100.10	0.63	3.64	8.29	0.083
18X-2, 50-52	151.11	22.10	30.20	40.90	83.40	276.16	0.49	42.50	37.74	0.137
18X-5, 50-52	154.96	17.52	24.70	25.10	40.50	163.97	0.62	15.40	23.12	0.141
19X-2, 50-52	159.01	14.99	15.30	15.60	21.50	140.52	0.73	5.90	14.34	0.102
19X-4, 50-52	162.01	13.49	13.30	9.05	14.60	109.77	0.62	5.55	10.82	0.099
20X-2, 46-48	168.47	11.96	9.02	4.54	7.24	80.27	0.63	2.70	6.05	0.075
20X-5, 56-58	173.07	11.13	6.00	2.11	3.22	53.67	0.66	1.11	2.89	0.054
21X-1, 47-49	176.58	11.43	7.97	3.69	5.84	73.27	0.63	2.15	5.11	0.070
21X-2, 50-52	178.11	3.73	4.40	1.98	3.28	74.55	0.60	1.30	8.80	0.118
21X-3, 58-60	179.61	8.58	7.98	3.86	5.91	74.06	0.65	2.05	6.89	0.093
21X-4, 50-52	181.01	7.68	11.10	5.57	8.64	77.84	0.64	3.07	11.25	0.145
21X-5, 51-53	182.04	13.43	11.00	6.42	9.56	86.91	0.67	3.14	7.12	0.082
22X-2, 50-52	187.41	11.85	0.00	5.75	9.08		0.63	3.33	7.66	0.000
22X-6, 50-52	193.41	11.41	5.83	2.20	3.44	59.01	0.64	1.24	3.02	0.051
23X-2, 50-52	196.71	13.61	8.23	5.53	9.39	114.09	0.59	3.86	6.90	0.060
23X-4, 50-52	199.71	13.33	9.40	5.75	9.49	100.96	0.61	3.74	7.12	0.071
24X-2, 50-52	206.21	14.50	0.00	0.00	0.00			0.00	0.00	0.000
24X-5, 50-52	210.71	12.77	9.09	4.56	7.17	78.88	0.64	2.61	5.62	0.071

Table T2 (continued).

Core, section, interval (cm)	Depth (mbsf)	$\chi$ ( $10^{-8} \text{ m}^3/\text{kg}$ )	ARM ( $10^{-6} \text{ Am}^2/\text{kg}$ )	IRM@0.1T ( $10^{-4} \text{ Am}^2/\text{kg}$ )	IRM@0.9T ( $10^{-4} \text{ Am}^2/\text{kg}$ )	IRM@0.9T/ ARM	IRM@0.1T/ IRM@0.9T	IRM@0.9T- IRM@0.1T ( $10^{-4} \text{ Am}^2/\text{kg}$ )	IRM@0.9T/ $\chi$ ( $10^3 \text{ A/m}$ )	ARM/ $\chi$ ( $10^3 \text{ A/m}$ )
26X-6, 21–22	230.78	43.16	71.60	99.80	220.00	307.26	0.45	120.20	50.97	0.166
27X-2, 63–65	235.44	13.56	23.80	31.80	54.10	227.31	0.59	22.30	39.90	0.176
27X-5, 50–52	239.81	60.49	90.50	100.00	329.54	364.13	0.30	229.54	54.48	0.150
28X-2, 51–53	244.94	19.72	23.20	33.00	67.20	289.66	0.49	34.20	34.08	0.118
28X-5, 50–52	249.44	21.73	28.40	46.00	86.30	303.87	0.53	40.30	39.72	0.131
29X-2, 50–52	254.61	15.62	14.60	15.90	32.10	219.86	0.50	16.20	20.55	0.093
29X-5, 50–52	259.11	19.07	24.00	41.00	81.90	341.25	0.50	40.90	42.96	0.126
30X-2, 52–54	264.23	28.78	45.90	86.30	157.00	342.05	0.55	70.70	54.55	0.159
30X-5, 117–119	269.35	38.79	79.70	160.00	261.00	327.48	0.61	101.00	67.29	0.205
31X-2, 52–54	272.93	15.47	14.50	15.60	30.60	211.03	0.51	15.00	19.77	0.094
31X-4, 51–53	276.53	28.78	48.20	87.50	154.00	319.50	0.57	66.50	53.51	0.167
32X-2, 109–111	284.1	28.46	49.20	91.10	157.00	319.11	0.58	65.90	55.16	0.173
34X-2, 50–52	295.21	44.60	62.30	138.00	222.00	356.34	0.62	84.00	49.77	0.140
34X-5, 50–52	299.71	26.99	46.80	89.40	156.00	333.33	0.57	66.60	57.80	0.173
35X-2, 51–53	302.82	22.45	37.70	63.40	105.00	278.51	0.60	41.60	46.78	0.168
35X-5, 51–53	307.32	20.78	25.30	44.30	87.70	346.64	0.51	43.40	42.21	0.122
36X-2, 57–59	312.48	18.61	20.20	33.80	63.60	314.85	0.53	29.80	34.18	0.109
36X-5, 50–52	316.91	31.63	44.80	97.20	168.00	375.00	0.58	70.80	53.12	0.142
37X-2, 53–55	322.04	48.38	71.40	178.00	294.00	411.76	0.61	116.00	60.77	0.148
37X-5, 50–52	326.51	24.90	38.50	76.60	151.00	392.21	0.51	74.40	60.64	0.155
38X-2, 50–52	331.71	15.02	17.90	23.10	40.30	225.14	0.57	17.20	26.83	0.119
38X-6, 62–64	337.83	25.66	49.30	82.40	142.00	288.03	0.58	59.60	55.35	0.192
39X-2, 50–52	341.21	56.60	71.50	174.00	326.00	455.94	0.53	152.00	57.59	0.126
39X-5, 62–64	345.76	42.75	52.30	125.00	232.00	443.59	0.54	107.00	54.27	0.122
40X-2, 40–42	350.81	33.69	44.40	91.60	170.00	382.88	0.54	78.40	50.46	0.132
40X-5, 27–29	355.15	17.55	19.10	25.10	45.20	236.65	0.56	20.10	25.76	0.109
41X-2, 68–70	360.69	15.40	16.50	25.50	47.50	287.88	0.54	22.00	30.84	0.107
42X-2, 50–52	370.21	50.49	78.70	165.00	293.00	372.30	0.56	128.00	58.04	0.156
42X-5, 50–52	374.69	24.80	42.50	76.80	126.00	296.47	0.61	49.20	50.81	0.171
43X-2, 59–61	379.9	38.23	53.40	124.00	212.00	397.00	0.58	88.00	55.45	0.140
43X-5, 50–52	384.31	43.90	51.30	130.00	243.00	473.68	0.53	113.00	55.36	0.117
4R-1, 50–52	501.41	25.90	47.20	88.30	135.00	286.02	0.65	46.70	52.12	0.182
5R-1, 50–52	511.01	20.78	38.70	67.20	110.00	284.24	0.61	42.80	52.93	0.186

Table T3. Rock magnetic data, Site 1246.

Core, section, interval (cm)	Depth (mbsf)	$\chi$ ( $10^{-8} \text{ m}^3/\text{kg}$ )	ARM ( $10^{-6} \text{ Am}^2/\text{kg}$ )	IRM@0.1T ( $10^{-4} \text{ Am}^2/\text{kg}$ )	IRM@0.9T ( $10^{-4} \text{ Am}^2/\text{kg}$ )	IRM@0.9T /ARM	IRM@0.1T/IRM@0.9T	IRM@0.9T-IRM@0.1T ( $10^{-4} \text{ Am}^2/\text{kg}$ )	IRM @0.9T/ $\chi$ ( $10^3 \text{ A/m}$ )	ARM/ $\chi$ ( $10^3 \text{ A/m}$ )
204-1247B-										
1H-1, 50-52	0.51	13.54	7.30	2.76	4.07	55.75	0.68	1.31	3.01	0.054
1H-2, 50-52	2.01	11.21	7.31	2.94	4.41	60.33	0.67	1.47	3.93	0.065
1H-3, 50-52	3.51	10.33	6.99	3.00	4.31	61.66	0.70	1.31	4.17	0.068
2H-1, 50-52	5.21	11.89	7.24	2.99	4.39	60.64	0.68	1.40	3.69	0.061
2H-2, 50-52	6.71	11.54	7.78	4.00	6.21	79.82	0.64	2.21	5.38	0.067
2H-3, 50-52	8.21	11.50	9.18	5.39	8.58	93.46	0.63	3.19	7.46	0.080
2H-4, 50-52	9.71	11.05	10.30	5.49	8.86	86.02	0.62	3.37	8.01	0.093
2H-5, 50-52	11.21	14.65	16.90	9.79	16.90	100.00	0.58	7.11	11.54	0.115
2H-6, 50-52	12.71	15.36	19.80	16.70	33.80	170.71	0.49	17.10	22.01	0.129
3H-1, 50-52	14.71	12.40	8.31	5.16	8.85	106.50	0.58	3.69	7.13	0.067
3H-2, 50-52	16.21	12.16	6.94	3.33	5.23	75.36	0.64	1.90	4.30	0.057
3H-3, 50-52	17.71	14.01	12.80	9.59	14.20	110.94	0.68	4.61	10.14	0.091
3H-4, 50-52	19.21	20.46	15.40	10.90	14.80	96.10	0.74	3.90	7.23	0.075
3H-5, 50-52	20.71	22.26	25.30	40.10	63.20	249.80	0.63	23.10	28.39	0.114
3H-6, 40-42	22.11	15.01	13.40	9.72	13.90	103.73	0.70	4.18	9.26	0.089
4H-2, 50-52	25.71	12.90	10.80	6.34	8.71	80.65	0.73	2.37	6.75	0.084
4H-5, 50-52	30.21	41.50	129.00	0.00	0.00	0.00	0.00	0.00	0.00	0.311
5H-1, 50-52	33.71	13.36	11.10	6.03	8.52	76.76	0.71	2.49	6.38	0.083
5H-5, 50-52	39.71	14.27	11.40	5.85	8.61	75.53	0.68	2.76	6.03	0.080
6H-2, 50-52	44.68	12.28	10.40	5.41	7.94	76.35	0.68	2.53	6.47	0.085
6H-5, 50-52	49.11	14.69	12.60	6.72	9.79	77.70	0.69	3.07	6.66	0.086
7H-1, 45-47	52.66	20.94	23.70	20.40	32.10	135.44	0.64	11.70	15.33	0.113
7H-2, 50-52	54.1	131.41	103.00	101.00	136.00	132.04	0.74	35.00	10.35	0.078
7H-3, 51-53	55.61	131.84	88.10	74.10	85.20	96.71	0.87	11.10	6.46	0.067
7H-4, 53-55	57.13	23.28	22.60	11.20	17.10	75.66	0.65	5.90	7.35	0.097
7H-5, 50-52	58.6	18.54	17.90	11.20	16.60	92.74	0.67	5.40	8.95	0.097
7H-6, 65-67	60.25	18.14	17.20	9.58	14.30	83.14	0.67	4.72	7.88	0.095
7H-7, 50-52	61.1	18.69	21.60	13.50	19.10	88.43	0.71	5.60	10.22	0.116
8H-1, 56-58	62.27	24.63	21.20	12.70	19.00	89.62	0.67	6.30	7.71	0.086
8H-2, 50-52	63.71	135.50	100.00	124.00	157.00	157.00	0.79	33.00	11.59	0.074
8H-3, 51-53	65.22	171.78	138.00	141.00	169.00	122.46	0.83	28.00	9.84	0.080
8H-4, 51-53	66.72	24.39	27.10	18.80	30.20	111.44	0.62	11.40	12.38	0.111
8H-5, 50-52	68.21	18.02	16.80	10.10	14.60	86.90	0.69	4.50	8.10	0.093
8H-6, 39-41	69.6	17.81	16.90	10.00	14.80	87.57	0.68	4.80	8.31	0.095
9H-2, 86-88	73.24	43.62	132.00	0.00	0.00	0.00	0.00	0.00	0.00	0.303
9H-5, 49-51	77.41	18.03	17.00	12.30	18.40	108.24	0.67	6.10	10.20	0.094
10H-2, 62-64	82.83	13.77	11.20	8.18	12.50	111.61	0.65	4.32	9.08	0.081
10H-5, 93-95	87.64	13.61	9.11	5.24	7.67	84.19	0.68	2.43	5.64	0.067
11H-1, 50-52	90.71	16.38	15.20	13.00	19.80	130.26	0.66	6.80	12.08	0.093
11H-2, 50-52	92.21	14.94	11.80	7.96	11.10	94.07	0.72	3.14	7.43	0.079
11H-3, 50-52	93.71	15.63	12.00	8.89	12.00	100.00	0.74	3.11	7.68	0.077
11H-4, 45-47	95.15	14.89	12.40	11.20	17.40	140.32	0.64	6.20	11.68	0.083
12H-1, 106-108	100.77	15.16	14.30	22.70	35.30	246.85	0.64	12.60	23.28	0.094
12H-2, 86-88	102.07	14.73	14.60	13.30	19.90	136.30	0.67	6.60	13.51	0.099
12H-3, 62-64	103.33	13.75	10.40	7.44	11.00	105.77	0.68	3.56	8.00	0.076
12H-4, 50-52	104.57	16.60	11.00	9.32	14.90	135.45	0.63	5.58	8.98	0.066
12H-5, 50-52	105.84	13.85	11.60	9.33	13.70	118.10	0.68	4.37	9.90	0.084
12H-6, 50-52	107.34	12.63	9.80	5.80	8.59	87.65	0.68	2.79	6.80	0.078
13H-2, 50-52	111.21	12.04	8.49	5.14	8.25	97.17	0.62	3.11	6.85	0.071
13H-5, 50-52	115.71	14.38	12.00	8.82	12.70	105.83	0.69	3.88	8.83	0.083
14H-1, 100-102	119.71	24.12	28.70	53.90	97.80	340.77	0.55	43.90	40.55	0.119
15H-2, 50-52	124.26	32.09	42.70	91.40	162.00	379.39	0.56	70.60	50.49	0.133
15H-5, 54-56	128.8	21.82	27.60	44.00	72.20	261.59	0.61	28.20	33.09	0.126
16H-2, 50-52	131.81	12.93	11.60	8.47	11.70	100.86	0.72	3.23	9.05	0.090
16H-5, 46-48	136.27	13.98	12.50	8.91	12.20	97.60	0.73	3.29	8.72	0.089

**Table T4.** Rock magnetic data, Site 1247.

Core, section, interval (cm)	Depth (mbsf)	$\chi$ ( $10^{-8} \text{ m}^3/\text{kg}$ )	ARM ( $10^{-6} \text{ Am}^2/\text{kg}$ )	IRM@0.1T ( $10^{-4} \text{ Am}^2/\text{kg}$ )	IRM@0.9T ( $10^{-4} \text{ Am}^2/\text{kg}$ )	IRM @0.9T/ARM	IRM@0.1T/IRM@0.9T	IRM@0.9T-IRM@0.1T ( $10^{-4} \text{ Am}^2/\text{kg}$ )	IRM@0.9 T/ $\chi$ ( $10^3 \text{ A/m}$ )	ARM/ $\chi$ ( $10^3 \text{ A/m}$ )
204-1247B-										
1H-1, 50-52	0.51	15.50	20.90	8.66	14.70	70.33	0.59	6.04	9.48	0.135
2H-1, 50-52	4.11	10.34	11.50	4.36	6.93	60.26	0.63	2.57	6.70	0.111
2H-2, 50-52	5.61	11.55	9.43	3.61	5.76	61.08	0.63	2.15	4.99	0.082
2H-3, 50-52	7.11	9.81	8.11	2.68	4.19	51.66	0.64	1.51	4.27	0.083
2H-4, 50-52	8.61	9.61	8.41	3.18	4.95	58.86	0.64	1.77	5.15	0.088
2H-5, 50-52	10.11	12.21	15.10	13.70	23.70	156.95	0.58	10.00	19.40	0.124
2H-6, 50-52	11.61	10.58	0.00	0.00	0.00			0.00	0.00	0.000
2H-7, 50-52	13.11	11.12	8.51	3.00	4.63	54.41	0.65	1.63	4.16	0.077
3H-2, 50-52	15.11	10.24	0.00	0.00	0.00			0.00	0.00	0.000
3H-5, 50-52	19.61	13.38	0.00	0.00	0.00			0.00	0.00	0.000
5H-1, 55-57	24.16	13.64	0.00	0.00	0.00			0.00	0.00	0.000
5H-5, 50-52	31.11	11.06	10.00	4.84	7.45	74.50	0.65	2.61	6.74	0.090
5H-6, 128-130	33.38	141.80	751.00	0.00	0.00			0.00	0.00	0.530
6H-2, 55-57	36.16	15.71	12.60	8.59	12.00	95.24	0.72	3.41	7.64	0.080
6H-5, 50-52	40.61	18.32	12.50	8.41	11.60	92.80	0.73	3.19	6.33	0.068
7H-2, 61-63	45.67	15.60	0.00	0.00	0.00			0.00	0.00	0.000
7H-5, 58-60	50.14	18.17	13.20	8.40	11.80	89.39	0.71	3.40	6.50	0.073
8H-2, 47-49	55.08	48.07	39.30	28.80	36.70	93.38	0.78	7.90	7.64	0.082
8H-4, 102-104	58.62	51.87	157.00	0.00	0.00			0.00	0.00	0.303
9H-2, 50-52	64.52	14.13	17.10	11.60	18.90	110.53	0.61	7.30	13.37	0.121
9H-5, 50-52	69.02	159.14	770.00	0.00	0.00			0.00	0.00	0.484
10H-2, 50-52	74.11	15.83	17.60	10.20	0.00			0.00	0.00	0.111
10H-5, 50-52	78.61	13.14	11.60	6.43	0.00			0.00	0.00	0.088
11H-2, 34-36	83.06	12.22	10.30	5.13	7.80	75.73	0.66	2.67	6.38	0.084
11H-5, 47-49	87.69	13.43	10.30	5.37	7.99	77.57	0.67	2.62	5.95	0.077
12H-2, 07-09	92.68	15.81	17.20	9.26	14.50	84.30	0.64	5.24	9.17	0.109
12H-5, 50-52	96.61	23.11	31.40	31.40	46.20	147.13	0.68	14.80	19.99	0.136
13H-1, 50-52	101.11	13.72	13.00	7.97	12.40	95.38	0.64	4.43	9.04	0.095
13H-2, 62-64	102.36	14.37	14.40	10.50	16.80	116.67	0.63	6.30	11.69	0.100
13H-3, 50-52	103.74	15.91	25.30	26.00	35.30	139.53	0.74	9.30	22.19	0.159
13H-4, 47-49	105.21	14.52	20.60	21.80	29.50	143.20	0.74	7.70	20.32	0.142
13H-5, 45-47	106.18	13.80	14.80	15.00	20.40	137.84	0.74	5.40	14.79	0.107
14H-1, 50-52	107.21	13.64	20.70	20.80	25.70	124.15	0.81	4.90	18.84	0.152
14H-2, 50-52	108.71	13.22	15.70	13.40	17.40	110.83	0.77	4.00	13.16	0.119
14H-3, 50-52	110.21	12.51	15.90	14.90	23.30	146.54	0.64	8.40	18.62	0.127
14H-4, 50-52	111.71	13.44	13.00	9.45	14.60	112.31	0.65	5.15	10.86	0.097
14H-5, 20-22	112.91	13.51	11.50	7.68	11.50	100.00	0.67	3.82	8.51	0.085
15X2, 50-52	115.61	12.79	11.20	6.69	9.94	88.75	0.67	3.25	7.77	0.088
18X2, 50-52	129.31	19.68	27.60	33.30	54.10	196.01	0.62	20.80	27.50	0.140
18X5, 50-52	133.81	21.22	38.00	84.30	170.00	447.37	0.50	85.70	80.12	0.179
19X2, 50-52	136.61	12.91	12.50	7.70	11.60	92.80	0.66	3.90	8.99	0.097
19X5, 50-52	141.08	13.00	8.15	3.96	5.75	70.55	0.69	1.79	4.42	0.063
20X1, 50-52	144.71	14.66	21.50	32.60	50.50	234.88	0.65	17.90	34.45	0.147
20X2, 50-52	146.21	13.22	19.50	27.20	40.60	208.21	0.67	13.40	30.70	0.147
20X3, 50-52	147.71	10.98	7.41	3.16	4.86	65.59	0.65	1.70	4.43	0.067
20X4, 50-52	149.21	11.84	9.12	5.16	8.14	89.25	0.63	2.98	6.87	0.077
20X5, 46-48	150.67	12.63	12.70	8.12	12.00	94.49	0.68	3.88	9.50	0.101
20X6, 50-52	151.3	12.98	11.20	7.80	12.30	109.82	0.63	4.50	9.48	0.086
21X2, 50-52	155.91	11.61	0.00	2.19	3.29		0.67	1.10	2.83	0.000
21X5, 50-52	160.41	11.98	7.91	0.00	0.00			0.00	0.00	0.066
22X2, 52-54	165.52	18.48	19.20	42.30	76.30	397.40	0.55	34.00	41.28	0.104
22X5, 48-50	169.99	25.50	63.20	158.00	173.20	274.05	0.91	15.20	67.91	0.248
23X2, 47-49	175.08	14.92	11.50	9.02	15.60	135.65	0.58	6.58	10.45	0.077
24X2, 50-52	184.71	25.88	49.90	72.50	106.00	212.42	0.68	33.50	40.96	0.193
24X5, 42-44	189.13	18.18	19.80	25.10	43.40	219.19	0.58	18.30	23.88	0.109
25X2, 70-72	194.24	13.62	9.25	5.97	9.70	104.86	0.62	3.73	7.12	0.068
25X6, 15-17	198.87	14.52	10.80	10.80	19.40	179.63	0.56	8.60	13.36	0.074
26X2, 50-52	203.91	18.83	25.10	36.20	58.80	234.26	0.62	22.60	31.22	0.133
26X5, 50-52	208.41	16.77	21.90	24.90	42.50	194.06	0.59	17.60	25.34	0.131
27X2, 47-49	213.18	15.44	18.10	21.20	35.80	197.79	0.59	14.60	23.18	0.117
27X5, 48-50	217.69	40.00	58.10	126.00	197.00	339.07	0.64	71.00	49.25	0.145

Table T5. Rock magnetic data, Site 1248.

Core, section, interval (cm)	Depth (mbsf)	$\chi$ ( $10^{-8} \text{ m}^3/\text{kg}$ )	ARM ( $10^{-6} \text{ Am}^2/\text{kg}$ )	IRM@0.1T ( $10^{-4} \text{ Am}^2/\text{kg}$ )	IRM@0.9T ( $10^{-4} \text{ Am}^2/\text{kg}$ )	IRM@0.9T/ ARM	IRM@0.1T/ IRM@0.9T	IRM@0.9T- IRM@0.1T ( $10^{-4} \text{ Am}^2/\text{kg}$ )	IRM@0.9T/ $\chi$ ( $10^3 \text{ A/m}$ )	ARM/ $\chi$ ( $10^3 \text{ A/m}$ )
204-1248C-										
1X-1, 50–52	0.51	13.64	11.10	5.14	7.57	68.20	0.68	2.43	5.55	0.081
3X-1, 73–75	19.94	18.02	13.20	9.08	13.20	100.00	0.69	4.12	7.32	0.073
3X-2, 63–65	21.34	33.48	71.70	153.00	229.00	319.39	0.67	76.00	68.40	0.214
3X-3, 4–6	21.88	34.13	71.70	123.00	174.00	242.68	0.71	51.00	50.98	0.210
3X-3, 49–51	22.33	31.94	50.30	85.00	123.00	244.53	0.69	38.00	38.51	0.157
3X-CC, 19–21	22.58	28.84	84.40	174.00	268.00	317.54	0.65	94.00	92.91	0.293
5X-1, 50–52	38.91	13.14	10.90	5.87	9.12	83.67	0.64	3.25	6.94	0.083
5X-2, 50–52	40.41	20.33	15.50	9.87	14.20	91.61	0.70	4.33	6.99	0.076
6H-2, 42–44	49.66	19.21	19.80	11.70	17.70	89.39	0.66	6.00	9.22	0.103
6H-5, 50–52	52.95	20.20	22.80	13.40	20.60	90.35	0.65	7.20	10.20	0.113
7H-2, 50–52	59.51	14.47	11.70	6.15	9.19	78.55	0.67	3.04	6.35	0.081
7H-5, 50–52	64.01	14.59	12.20	7.81	11.80	96.72	0.66	3.99	8.09	0.084
8H-2, 50–52	69.01	14.13	11.10	7.64	11.70	105.41	0.65	4.06	8.28	0.079
8H-5, 50–52	73.41	14.53	10.00	5.99	9.14	91.40	0.66	3.15	6.29	0.069
9H-2, 89–91	78.9	12.36	9.87	5.49	8.31	84.19	0.66	2.82	6.72	0.080
9H-5, 50–52	83.01	14.01	12.90	12.10	16.80	130.23	0.72	4.70	11.99	0.092
10H-2, 48–50	87.68	12.69	9.42	5.16	7.44	78.98	0.69	2.28	5.86	0.074
10H-5, 58–60	92.2	14.96	13.20	11.60	19.30	146.21	0.60	7.70	12.90	0.088
11H-2, 50–52	96.67	10.00	5.61	2.14	3.14	55.97	0.68	1.00	3.14	0.056
11H-5, 25–27	100.8	12.31	11.10	8.69	14.40	129.73	0.60	5.71	11.69	0.090
12H-2, 45–47	106.96	15.66	15.00	12.80	21.90	146.00	0.58	9.10	13.98	0.096
12H-5, 50–52	111.12	16.59	11.20	7.66	11.40	101.79	0.67	3.74	6.87	0.068
13H-1, 50–52	115.01	14.80	12.00	7.46	11.40	95.00	0.65	3.94	7.70	0.081
13H-2, 46–48	116.42	12.91	10.20	6.11	8.98	88.04	0.68	2.87	6.95	0.079
13H-3, 52–54	117.99	12.37	8.24	4.46	6.70	81.31	0.67	2.24	5.42	0.067
13H-4, 37–39	119.3	12.66	10.60	5.40	7.96	75.09	0.68	2.56	6.29	0.084
13H-5, 51–53	120.88	14.18	12.40	8.24	12.50	100.81	0.66	4.26	8.81	0.087
14H-1, 20–22	124.21	12.89	8.46	4.26	6.15	72.70	0.69	1.89	4.77	0.066
14H-2, 50–52	124.78	12.87	9.07	4.49	6.46	71.22	0.70	1.97	5.02	0.070
14H-3, 50–52	126.28	12.76	10.30	5.75	8.47	82.23	0.68	2.72	6.64	0.081
14H-4, 51–53	127.76	14.73	10.90	6.37	9.80	89.91	0.65	3.43	6.65	0.074
14H-5, 50–52	129.25	11.85	8.79	4.55	6.38	72.58	0.71	1.83	5.38	0.074
14H-6, 47–49	130.72	1.82	4.64	2.13	3.21	69.18	0.66	1.08	17.63	0.255
15H-1, 41–43	133.94	11.81	6.16	2.27	3.47	56.33	0.65	1.20	2.94	0.052
15H-2, 54–56	134.96	11.86	8.44	3.69	5.50	65.17	0.67	1.81	4.64	0.071
15H-3, 48–50	135.96	11.83	8.01	3.63	5.38	67.17	0.67	1.75	4.55	0.068
16H-1, 20–22	137.01	14.04	11.90	8.61	14.20	119.33	0.61	5.59	10.11	0.085
16H-2, 50–52	138.51	19.77	28.50	48.50	75.80	265.96	0.64	27.30	38.34	0.144
16H-3, 50–52	140.01	14.13	10.50	6.92	11.10	105.71	0.62	4.18	7.85	0.074
16H-4, 50–52	141.54	14.15	10.60	6.39	9.93	93.68	0.64	3.54	7.02	0.075
17X-2, 50–52	143.96	13.72	10.80	6.87	11.30	104.63	0.61	4.43	8.23	0.079
17X-5, 50–52	147.96	15.20	12.50	9.70	16.20	129.60	0.60	6.50	10.66	0.082

**Table T6.** Rock magnetic data, Site 1249.

Core, section, interval (cm)	Depth (mbsf)	$\chi$ ( $10^{-8} \text{ m}^3/\text{kg}$ )	ARM ( $10^{-6} \text{ Am}^2/\text{kg}$ )	IRM@0.1T ( $10^{-4} \text{ Am}^2/\text{kg}$ )	IRM@0.9T ( $10^{-4} \text{ Am}^2/\text{kg}$ )	IRM@0.9T/ ARM	IRM@0.1T/ IRM@0.9T	IRM@0.9T- IRM@0.1T ( $10^{-4} \text{ Am}^2/\text{kg}$ )	IRM@0.9T/ $\chi$ ( $10^3 \text{ A/m}$ )	ARM/ $\chi$ ( $10^3 \text{ A/m}$ )
204-1249C-										
1H-1, 67–69	0.68	14.46	12.90	4.00	5.87	45.50	0.68	1.87	4.06	0.089
2H-1, 50–52	2.51	19.20	11.20	5.79	8.57	76.52	0.68	2.78	4.46	0.058
3H-1, 50–52	5.51	12.32	10.70	5.56	8.87	82.90	0.63	3.31	7.20	0.087
4H-2, 6–8	15.4	16.50	15.90	7.82	10.80	67.92	0.72	2.98	6.55	0.096
4H-5, 50–52	17.26	19.26	15.40	8.20	11.60	75.32	0.71	3.40	6.02	0.080
5H-3, 10–12	26.26	15.73	11.30	8.18	12.40	109.73	0.66	4.22	7.89	0.072
5H-6, 50–52	29.22	15.42	9.65	5.46	7.49	77.62	0.73	2.03	4.86	0.063
204-1249B-										
2H-2, 29–31	31.8	7.67	5.20	2.67	4.22	81.15	0.63	1.55	5.50	0.068
204-1249C-										
7H-1, 85–87	35.86	15.87	13.30	7.84	11.60	87.22	0.68	3.76	7.31	0.084
7H-2, 50–52	36.47	15.95	13.90	12.20	20.50	147.48	0.60	8.30	12.85	0.087
7H-5, 50–52	38.64	15.93	11.80	7.52	10.90	92.37	0.69	3.38	6.84	0.074
7H-5, 90–92	39.04	15.70	13.90	9.82	15.20	109.35	0.65	5.38	9.68	0.089
8H-3, 32–34	44.82	15.02	11.30	6.98	9.80	86.73	0.71	2.82	6.53	0.075
8H-4, 60–62	49.55	25.51	36.30	105.00	197.00	542.70	0.53	92.00	77.24	0.142
8H-4, 138–140	50.33	18.39	22.30	26.50	41.40	185.65	0.64	14.90	22.51	0.121
9H-2, 50–52	56.01	16.77	13.90	10.30	15.50	111.51	0.66	5.20	9.24	0.083
9H-4, 50–52	58.84	13.75	9.17	4.13	6.25	68.16	0.66	2.12	4.54	0.067
11H-2, 46–48	66.62	23.69	28.50	18.10	27.00	94.74	0.67	8.90	11.40	0.120
11H-5, 50–52	69.93	22.45	34.50	49.40	78.20	226.67	0.63	28.80	34.83	0.154
11H-4, 118–120	70.3	20.13	20.20	11.60	17.30	85.64	0.67	5.70	8.59	0.100
12H-2, 50–52	76.41	15.93	11.10	6.44	9.64	86.85	0.67	3.20	6.05	0.070
12H-2, 139–141	77.5	11.52	7.94	3.89	5.51	69.40	0.71	1.62	4.78	0.069
13H-2, 50–52	86.01	39.12	111.00	182.32	347.05	312.66	0.53	164.73	88.71	0.284
13H-5, 50–52	89.42	15.66	13.40	10.40	16.80	125.37	0.62	6.40	10.73	0.086

Table T7. Rock magnetic data, Site 1250.

Core, section, interval (cm)	Depth (mbsf)	$\chi$ ( $10^{-8} \text{ m}^3/\text{kg}$ )	ARM ( $10^{-6} \text{ Am}^2/\text{kg}$ )	IRM@0.1T ( $10^{-4} \text{ Am}^2/\text{kg}$ )	IRM@0.9T ( $10^{-4} \text{ Am}^2/\text{kg}$ )	IRM@0.9T/ ARM	IRM@0.9T/ IRM@0.9T	IRM@0.1T/ IRM@0.9T ( $10^{-4} \text{ Am}^2/\text{kg}$ )	IRM@0.9T/ $\chi$ ( $10^3 \text{ A/m}$ )	ARM/ $\chi$ ( $10^3 \text{ A/m}$ )
204-1250C-										
3H-2, 50-52	16.01	16.81	15.40	15.10	20.80	135.06	0.73	5.70	12.37	0.092
3H-5, 50-52	20.51	16.33	12.10	7.46	11.40	94.21	0.65	3.94	6.98	0.074
4H-2, 50-52	25.51	19.06	16.40	12.30	19.40	118.29	0.63	7.10	10.18	0.086
4H-5, 50-52	29.61	18.48	12.50	8.33	11.80	94.40	0.71	3.47	6.39	0.068
5H-2, 50-52	34.99	13.82	11.40	5.45	8.24	72.28	0.66	2.79	5.96	0.082
5H-5, 50-52	39.49	13.68	8.57	3.64	5.63	65.69	0.65	1.99	4.11	0.063
6H-2, 50-52	44.51	16.69	10.30	6.28	8.66	84.08	0.73	2.38	5.19	0.062
6H-5, 54-56	48.32	27.56	33.20	46.50	68.10	205.12	0.68	21.60	24.71	0.120
7H-2, 50-52	54.01	16.23	12.40	7.30	10.90	87.90	0.67	3.60	6.71	0.076
7H-5, 50-52	57.21	17.33	14.20	9.77	14.40	101.41	0.68	4.63	8.31	0.082
8H-2, 50-52	63.51	28.14	76.10	176.00	234.00	307.49	0.75	58.00	83.16	0.270
8H-5, 50-52	68.01	17.09	22.10	16.50	24.50	110.86	0.67	8.00	14.33	0.129
10H-2, 65-67	75.16	14.42	10.10	6.18	9.94	98.42	0.62	3.76	6.89	0.070
10H-5, 53-55	79	14.74	9.37	5.44	8.44	90.07	0.64	3.00	5.72	0.064
11H-1, 50-52	83.01	14.20	16.80	32.30	49.10	292.26	0.66	16.80	34.58	0.118
11H-2, 49-51	84.46	13.34	10.00	6.42	9.74	97.40	0.66	3.32	7.30	0.075
11H-3, 47-49	85.89	14.35	12.30	10.30	16.40	133.33	0.63	6.10	11.43	0.086
11H-4, 50-52	87.02	13.60	7.90	3.42	5.18	65.57	0.66	1.76	3.81	0.058
11H-5, 49-51	88.51	14.38	9.62	5.36	7.62	79.21	0.70	2.26	5.30	0.067
11H-6, 50-52	89.97	13.53	7.94	2.94	4.27	53.78	0.69	1.33	3.16	0.059
12H-2, 48-50	93.14	12.91	8.57	3.76	5.68	66.28	0.66	1.92	4.40	0.066
12H-5, 50-52	97.54	11.10	5.46	1.82	2.80	51.28	0.65	0.98	2.52	0.049
13H-3, 42-44	103.82	12.38	7.66	4.11	6.45	84.20	0.64	2.34	5.21	0.062
13H-5, 60-62	107	14.17	11.50	7.55	12.80	111.30	0.59	5.25	9.03	0.081
14H-1, 130-132	112.31	16.02	9.92	7.44	12.70	128.02	0.59	5.26	7.93	0.062
14H-2, 50-52	113.01	17.59	13.40	10.90	17.70	132.09	0.62	6.80	10.06	0.076
14H-3, 44-46	114.45	16.40	10.50	6.01	9.24	88.00	0.65	3.23	5.64	0.064
14H-4, 33-35	115.27	14.69	9.00	6.15	9.51	105.67	0.65	3.36	6.47	0.061
15H-2, 54-56	122.41	15.55	9.61	7.38	13.60	141.52	0.54	6.22	8.75	0.062
15H-5, 50-52	126.57	52.42	187.00	280.99	357.90	191.39	0.79	76.91	68.27	0.357
17H-2, 50-52	134.01	15.91	14.60	9.69	14.40	98.63	0.67	4.71	9.05	0.092
17H-4, 50-52	137.01	16.37	12.60	8.89	14.00	111.11	0.64	5.11	8.55	0.077
19X-2, 50-52	140.51	14.44	9.18	4.44	6.56	71.46	0.68	2.12	4.54	0.064
19X-5, 50-52	144.96	16.38	16.10	14.50	25.00	155.28	0.58	10.50	15.27	0.098

**Table T8.** Rock magnetic data, Site 1251. (Continued on next page.)

Core, section, interval (cm)	Depth (mbsf)	$\chi$ ( $10^{-8}$ m <sup>3</sup> /kg)	ARM ( $10^{-6}$ Am <sup>2</sup> /kg)	IRM@0.1T ( $10^{-4}$ Am <sup>2</sup> /kg)	IRM@0.9T ( $10^{-4}$ Am <sup>2</sup> /kg)	IRM@0.9T/ ARM	IRM@0.1T/ IRM@0.9T	IRM@0.9T- IRM@0.1T ( $10^{-4}$ Am <sup>2</sup> /kg)	IRM@0.9T/ $\chi$ ( $10^3$ A/m)	ARM/ $\chi$ ( $10^3$ A/m)
204-1251B-										
1H-2, 50-52	2.01	12.18	9.30	3.54	5.08	54.62	0.70	1.54	4.17	0.076
1H-5, 50-52	6.51	12.33	9.41	3.59	5.38	57.17	0.67	1.79	4.36	0.076
3H-2, 50-52	20.54	63.74	47.30	42.00	52.60	111.21	0.80	10.60	8.25	0.074
3H-5, 19-21	24.71	37.59	26.40	22.10	27.60	104.55	0.80	5.50	7.34	0.070
4H-2, 50-52	30.11	26.14	16.50	11.00	14.40	87.27	0.76	3.40	5.51	0.063
4H-4, 50-52	33.11	30.05	19.70	14.30	18.10	91.88	0.79	3.80	6.02	0.066
5H-2, 50-52	39.61	19.95	13.10	9.11	11.80	90.08	0.77	2.69	5.91	0.066
5H-5, 50-52	43.97	16.39	11.60	6.85	10.10	87.07	0.68	3.25	6.16	0.071
6H-2, 53-54	48.46	12.53	9.68	4.92	8.07	83.37	0.61	3.15	6.44	0.077
6H-5, 50-52	52.81	13.03	10.20	4.70	7.28	71.37	0.65	2.58	5.59	0.078
7H-2, 50-52	58.61	14.22	9.18	5.35	7.54	82.14	0.71	2.19	5.30	0.065
7H-5, 50-52	63.11	15.72	10.80	5.88	8.42	77.96	0.70	2.54	5.36	0.069
8H-2, 50-52	68.11	14.71	12.40	6.04	9.17	73.95	0.66	3.13	6.23	0.084
10H-2, 50-52	87.11	16.37	9.56	6.75	9.20	96.23	0.73	2.45	5.62	0.058
10H-5, 50-52	91.61	17.59	10.80	7.80	10.20	94.44	0.76	2.40	5.80	0.061
11H-2, 51-53	96.62	20.26	13.60	9.79	13.00	95.59	0.75	3.21	6.42	0.067
11H-5, 50-52	100.55	14.19	9.74	5.49	8.46	86.86	0.65	2.97	5.96	0.069
13H-2, 50-52	107.76	18.01	10.90	8.94	11.70	107.34	0.76	2.76	6.50	0.061
13H-5, 66-68	112.22	18.31	12.10	9.16	12.10	100.00	0.76	2.94	6.61	0.066
14H-2, 50-52	117.12	13.15	7.28	2.93	4.33	59.48	0.68	1.40	3.29	0.055
14H-5, 50-52	121.62	13.49	8.91	3.74	5.60	62.85	0.67	1.86	4.15	0.066
15H-2, 59-61	127.2	21.36	13.90	9.52	12.20	87.77	0.78	2.68	5.71	0.065
15H-5, 50-52	131.61	15.46	12.20	5.58	8.45	69.26	0.66	2.87	5.47	0.079
16H-2, 73-75	136.84	12.54	6.35	2.55	3.82	60.16	0.67	1.27	3.05	0.051
16H-5, 50-52	141.11	13.87	7.72	3.11	4.45	57.64	0.70	1.34	3.21	0.056
17H-2, 50-52	146.11	33.92	30.90	20.70	28.40	91.91	0.73	7.70	8.37	0.091
17H-5, 50-52	150.61	14.18	7.15	2.99	4.50	62.94	0.66	1.51	3.17	0.050
19H-2, 83-85	157.7	13.23	8.44	3.76	5.86	69.43	0.64	2.10	4.43	0.064
19H-5, 50-52	161.79	15.29	10.70	5.80	8.03	75.05	0.72	2.23	5.25	0.070
20H-2, 50-52	165.19	16.95	12.90	8.94	12.90	100.00	0.69	3.96	7.61	0.076
20H-5, 52-54	169.71	18.70	16.00	8.23	11.80	73.75	0.70	3.57	6.31	0.086
22H-2, 64-66	174.85	16.85	9.00	5.96	8.34	92.67	0.71	2.38	4.95	0.053
22H-5, 18-20	178.87	15.81	9.78	6.07	8.85	90.49	0.69	2.78	5.60	0.062
23X-1, 40-42	179.51	18.47	14.80	9.18	12.70	85.81	0.72	3.52	6.87	0.080
23X-2, 40-42	181.01	15.88	9.58	5.56	7.99	83.40	0.70	2.43	5.03	0.060
23X-3, 40-42	182.48	15.54	7.78	4.52	6.24	80.21	0.72	1.72	4.02	0.050
23X-4, 40-42	183.98	17.17	9.80	6.81	8.91	90.92	0.76	2.10	5.19	0.057
23H-2, 50-52	184.21	14.57	6.28	2.65	4.09	65.13	0.65	1.44	2.81	0.043
23X-5, 50-52	185.08	16.24	8.74	6.11	7.91	90.50	0.77	1.80	4.87	0.054
23H-5, 50-52	188.42	13.98	8.23	4.18	6.79	82.50	0.62	2.61	4.86	0.059
24X-1, 92-94	189.52	18.72	15.60	10.00	15.00	96.15	0.67	5.00	8.01	0.083
24X-2, 96-98	190.59	13.36	6.61	3.08	4.60	69.59	0.67	1.52	3.44	0.049
24X-3, 108-110	192.21	14.50	0.00	0.00	0.00			0.00	0.00	0.000
24X-4, 34-36	192.96	16.18	9.43	5.98	8.17	86.64	0.73	2.19	5.05	0.058
24X-5, 34-36	193.59	16.92	10.00	6.87	9.48	94.80	0.72	2.61	5.60	0.059
24X-6, 77-79	195.45	13.76	7.57	3.79	5.84	77.15	0.65	2.05	4.24	0.055
25X-1, 50-52	198.71	13.28	5.94	2.54	4.00	67.34	0.64	1.46	3.01	0.045
25X-2, 50-52	200.21	13.58	5.82	2.18	3.43	58.93	0.64	1.25	2.53	0.043
25X-3, 50-52	201.71	13.44	5.64	2.16	3.27	57.98	0.66	1.11	2.43	0.042
25X-4, 50-52	203.21	13.62	6.49	2.49	3.74	57.63	0.67	1.25	2.75	0.048
26X-2, 50-52	206.21	16.64	11.10	6.29	9.74	87.75	0.65	3.45	5.85	0.067
25X-6, 50-52	206.21	14.87	12.60	5.40	8.90	70.63	0.61	3.50	5.99	0.085
26X-5, 50-52	210.58	14.93	8.38	4.39	6.65	79.36	0.66	2.26	4.45	0.056
27X-2, 50-52	215.51	13.56	6.90	2.71	4.43	64.20	0.61	1.72	3.27	0.051
27X-5, 50-52	220.01	13.77	6.67	2.83	4.61	69.12	0.61	1.78	3.35	0.048
28X-2, 50-52	225.11	15.40	4.90	1.66	2.76	56.33	0.60	1.10	1.79	0.032
28X-5, 50-52	229.61	13.13	7.64	2.86	4.59	60.08	0.62	1.73	3.49	0.058
29X-2, 50-52	234.81	13.06	9.72	3.92	6.39	65.74	0.61	2.47	4.89	0.074
29X-4, 50-52	237.81	13.46	8.95	4.16	6.53	72.96	0.64	2.37	4.85	0.066
30X-2, 50-52	244.41	13.11	7.63	3.38	5.32	69.72	0.64	1.94	4.06	0.058
30X-4, 50-52	247.41	14.73	9.87	5.13	8.13	82.37	0.63	3.00	5.52	0.067
31X-2, 48-50	254.09	12.35	9.27	3.85	5.89	63.54	0.65	2.04	4.77	0.075
32X-2, 50-52	263.71	12.35	7.46	3.00	5.36	71.85	0.56	2.36	4.34	0.060
32X-5, 50-52	268.1	14.11	5.64	1.84	2.81	49.82	0.65	0.97	1.99	0.040
33X-2, 51-53	273.31	11.93	6.37	2.14	3.63	56.99	0.59	1.49	3.04	0.053
33X-4, 51-53	276.32	12.74	9.53	3.85	6.76	70.93	0.57	2.91	5.31	0.075
34X-2, 49-51	283	11.42	9.33	3.44	6.06	64.95	0.57	2.62	5.31	0.082

Table T8 (continued).

Core, section, interval (cm)	Depth (mbsf)	$\chi$ ( $10^{-8} \text{ m}^3/\text{kg}$ )	ARM ( $10^{-6} \text{ Am}^2/\text{kg}$ )	IRM@0.1T ( $10^{-4} \text{ Am}^2/\text{kg}$ )	IRM@0.9T ( $10^{-4} \text{ Am}^2/\text{kg}$ )	IRM@0.9T/ ARM	IRM@0.1T/ IRM@0.9T	IRM@0.9T- IRM@0.1T ( $10^{-4} \text{ Am}^2/\text{kg}$ )	IRM@0.9T/ $\chi$ ( $10^3 \text{ A/m}$ )	ARM/ $\chi$ ( $10^3 \text{ A/m}$ )
34X-5, 52–54	287.36	12.24	6.18	2.13	3.68	59.55	0.58	1.55	3.01	0.050
36X-2, 50–52	294.61	13.14	6.40	2.07	3.39	52.97	0.61	1.32	2.58	0.049
36X-5, 50–52	299.11	13.63	7.82	2.72	4.51	57.67	0.60	1.79	3.31	0.057
37X-2, 50–52	302.61	14.96	7.11	2.52	4.32	60.76	0.58	1.80	2.89	0.048
37X-5, 51–53	307.12	13.17	6.46	2.15	3.32	51.39	0.65	1.17	2.52	0.049
38X-2, 56–58	312.37	14.46	14.20	6.98	11.70	82.39	0.60	4.72	8.09	0.098
38X-5, 46–48	316.77	16.52	16.60	6.98	11.90	71.69	0.59	4.92	7.20	0.100
39X-2, 82–84	322.23	12.81	7.96	2.72	0.00			0.00	0.00	0.062
39X-5, 68–70	326.59	13.47	10.70	5.91	8.19	76.54	0.72	2.28	6.08	0.079
41X-2, 50–52	332.61	10.44	6.04	2.28	3.48	57.62	0.66	1.20	3.33	0.058
41X-5, 50–52	337.11	12.34	7.88	3.96	6.12	77.66	0.65	2.16	4.96	0.064
42X-2, 88–90	341.59	12.89	11.20	6.58	10.30	91.96	0.64	3.72	7.99	0.087
42X-5, 65–67	345.86	28.12	79.30	92.20	123.00	155.11	0.75	30.80	43.74	0.282
43X-2, 50–52	350.81	12.60	9.62	3.92	5.99	62.27	0.65	2.07	4.75	0.076
43X-5, 50–52	355.28	12.05	9.71	5.71	8.74	90.01	0.65	3.03	7.25	0.081
44X-2, 62–64	360.53	11.73	8.38	3.35	5.05	60.26	0.66	1.70	4.31	0.071
44X-5, 124–126	365.65	14.04	9.50	3.68	5.84	61.47	0.63	2.16	4.16	0.068
45X-2, 53–55	370.02	16.11	13.20	7.56	12.00	90.91	0.63	4.44	7.45	0.082
46X-2, 54–56	379.65	16.11	10.60	5.89	9.27	87.45	0.64	3.38	5.75	0.066
46X-5, 50–52	384.11	17.32	21.50	11.40	20.50	95.35	0.56	9.10	11.84	0.124
47X-2, 50–52	389.31	13.69	7.97	3.16	5.16	64.74	0.61	2.00	3.77	0.058
47X-5, 50–52	393.81	12.93	10.80	6.26	10.10	93.52	0.62	3.84	7.81	0.083
49X-2, 49–51	399.9	16.56	11.40	5.60	8.55	75.00	0.65	2.95	5.16	0.069
49X-5, 21–23	404.12	13.17	7.97	2.92	4.87	61.10	0.60	1.95	3.70	0.061
50X-2, 48–50	408.49	13.47	9.57	5.31	8.65	90.39	0.61	3.34	6.42	0.071
50X-5, 53–55	413.04	12.96	8.08	3.19	5.52	68.32	0.58	2.33	4.26	0.062
51X-2, 62–64	418.33	13.90	9.20	4.39	7.39	80.33	0.59	3.00	5.32	0.066
51X-4, 120–122	421.91	27.56	73.30	71.50	106.00	144.61	0.67	34.50	38.46	0.266
52X-2, 50–52	427.81	27.50	81.30	98.60	138.00	169.74	0.71	39.40	50.18	0.296
52X-5, 53–55	432.34	11.80	8.69	4.14	6.98	80.32	0.59	2.84	5.92	0.074
53X-2, 10–12	437.09	14.06	17.10	11.20	16.80	98.25	0.67	5.60	11.95	0.122
53X-5, 26–28	440.98	81.68	334.00	0.00	0.00			0.00	0.00	0.409

Table T9. Rock magnetic data, Site 1252. (Continued on next page.)

Core, section, interval (cm)	Depth (mbfs)	$\chi$ ( $10^{-8}$ m <sup>3</sup> /kg)	ARM ( $10^{-6}$ Am <sup>2</sup> /kg)	IRM@0.1T ( $10^{-4}$ Am <sup>2</sup> /kg)	IRM@0.9T ( $10^{-4}$ Am <sup>2</sup> /kg)	IRM@0.9T/ ARM	IRM@0.1T/ IRM@0.9T	IRM@0.9T- IRM@0.1T ( $10^{-4}$ Am <sup>2</sup> /kg)	IRM@0.9T/ $\chi$ ( $10^3$ A/m)	ARM/ $\chi$ ( $10^3$ A/m)
204-1252A-										
1H-1, 43–45	0.44	12.96	12.30	5.03	8.31	67.56	0.61	3.28	6.41	0.095
1H-2, 58–60	2.09	11.05	15.40	9.97	16.10	104.55	0.62	6.13	14.57	0.139
1H-3, 58–60	3.59	12.31	17.60	7.95	14.50	82.39	0.55	6.55	11.78	0.143
1H-4, 52–54	4.53	11.37	14.50	5.89	10.60	73.10	0.56	4.71	9.32	0.127
2H-1, 86–88	5.77	10.38	9.45	3.47	5.83	61.69	0.60	2.36	5.62	0.091
2H-2, 50–52	6.91	9.95	8.87	3.23	5.27	59.41	0.61	2.04	5.30	0.089
2H-3, 64–66	8.55	10.11	9.70	3.60	5.81	59.90	0.62	2.21	5.75	0.096
2H-4, 50–52	9.91	10.72	9.46	3.63	5.94	62.79	0.61	2.31	5.54	0.088
2H-5, 50–52	11.41	10.65	9.65	3.76	6.25	64.77	0.60	2.49	5.87	0.091
2H-6, 52–54	12.93	11.11	12.40	6.10	10.50	84.68	0.58	4.40	9.45	0.112
2H-7, 24–26	14.15	8.33	7.32	2.77	4.43	60.52	0.63	1.66	5.32	0.088
3H-2, 50–52	15.16	9.95	8.52	3.16	5.11	59.98	0.62	1.95	5.13	0.086
3H-3, 50–52	16.66	9.84	7.80	2.76	4.39	56.28	0.63	1.63	4.46	0.079
3H-4, 50–52	18.16	10.24	8.74	3.52	5.35	61.21	0.66	1.83	5.23	0.085
3H-5, 61–63	19.77	10.31	8.62	3.23	4.99	57.89	0.65	1.76	4.84	0.084
3H-6, 87–89	21.53	10.97	10.40	4.57	6.83	65.67	0.67	2.26	6.23	0.095
3H-7, 93–95	23.09	17.43	14.50	9.03	12.70	87.59	0.71	3.67	7.29	0.083
4H-1, 50–52	24.41	26.50	19.40	14.10	18.70	96.39	0.75	4.60	7.06	0.073
4H-2, 50–52	25.91	16.59	13.70	8.04	11.70	85.40	0.69	3.66	7.05	0.083
4H-3, 50–52	27.41	35.67	32.10	21.80	28.30	88.16	0.77	6.50	7.93	0.090
4H-4, 50–52	28.79	30.94	25.20	18.80	25.70	101.98	0.73	6.90	8.31	0.081
4H-5, 107–109	30.86	32.01	29.10	20.70	29.80	102.41	0.69	9.10	9.31	0.091
4H-6, 50–52	31.79	13.79	14.70	9.19	13.80	93.88	0.67	4.61	10.00	0.107
4H-7, 50–52	33.29	11.85	10.50	4.78	7.81	74.38	0.61	3.03	6.59	0.089
5H-1, 50–52	33.91	11.72	12.30	11.80	12.30	100.00	0.96	0.50	10.50	0.105
5H-2, 50–52	34.5	10.97	8.94	4.07	6.47	72.37	0.63	2.40	5.90	0.082
5H-3, 30–32	35.81	11.16	8.03	3.76	6.01	74.84	0.63	2.25	5.39	0.072
5H-4, 43–45	37.43	10.36	8.28	4.09	6.33	76.45	0.65	2.24	6.11	0.080
5H-5, 25–27	38.75	11.22	7.47	3.67	5.78	77.38	0.63	2.11	5.15	0.067
5H-5, 40–42	38.9	11.33	7.69	3.85	6.07	78.93	0.63	2.22	5.36	0.068
5H-6, 17–19	40.17	12.17	8.83	4.21	7.36	83.35	0.57	3.15	6.05	0.073
5H-7, 53–55	42.03	11.66	7.77	3.66	5.53	71.17	0.66	1.87	4.74	0.067
5H-8, 22–24	42.72	15.60	11.60	8.08	11.80	101.72	0.68	3.72	7.57	0.074
6H-1, 50–52	43.41	29.85	18.70	15.20	19.60	104.81	0.78	4.40	6.57	0.063
6H-2, 50–52	44.912	23.12	16.00	12.40	17.10	106.88	0.73	4.70	7.39	0.069
6H-3, 50–52	46.41	11.51	10.60	5.58	8.81	83.11	0.63	3.23	7.66	0.092
6H-4, 50–52	47.91	11.30	9.64	4.80	7.71	79.98	0.62	2.91	6.82	0.085
6H-5, 50–52	49.41	11.02	9.47	3.79	6.27	66.21	0.60	2.48	5.69	0.086
6H-6, 50–52	50.91	10.79	7.95	3.09	5.25	66.04	0.59	2.16	4.87	0.074
6H-7, 50–52	52.41	10.22	0.00	0.00	0.00	0.00	0.00	0.00	0.00	0.000
7H-2, 50–52	54.41	10.86	7.10	2.67	4.20	59.15	0.64	1.53	3.87	0.065
7H-5, 50–52	58.91	20.73	12.80	10.20	13.50	105.47	0.76	3.30	6.51	0.062
8H-2, 50–52	63.91	12.02	8.11	3.70	5.80	71.52	0.64	2.10	4.83	0.067
8H-5, 50–52	68.41	11.51	7.57	2.82	4.50	59.45	0.63	1.68	3.91	0.066
9H-3, 60–62	75.01	56.12	43.90	36.00	46.40	105.69	0.78	10.40	8.27	0.078
9H-5, 68–70	78.09	41.59	37.70	30.40	39.50	104.77	0.77	9.10	9.50	0.091
10H-1, 50–52	81.41	13.24	10.70	5.76	8.06	75.33	0.71	2.30	6.09	0.081
10H-5, 50–52	86.51	27.46	20.50	15.50	19.50	95.12	0.79	4.00	7.10	0.075
11H-2, 48–50	92.39	11.13	6.38	2.27	3.59	56.27	0.63	1.32	3.23	0.057
11H-5, 50–52	96.91	14.12	9.33	4.27	6.56	70.31	0.65	2.29	4.65	0.066
12H-2, 50–52	101.91	22.29	18.40	13.70	19.10	103.80	0.72	5.40	8.57	0.083
12H-5, 50–52	106.31	29.76	25.00	19.30	26.10	104.40	0.74	6.80	8.77	0.084
13H-2, 50–52	111.41	38.83	33.90	26.00	34.70	102.36	0.75	8.70	8.94	0.087
13H-5, 50–52	115.28	24.74	4.51	1.38	1.90	42.13	0.73	0.52	0.77	0.018
14H-2, 61–63	121.02	11.43	8.40	2.80	4.34	51.67	0.65	1.54	3.80	0.073
14H-6, 46–48	126.56	10.38	8.25	2.99	5.12	62.06	0.58	2.13	4.93	0.079
15H-2, 50–52	127.01	10.70	8.87	3.30	5.36	60.43	0.62	2.06	5.01	0.083
15H-5, 50–52	131.38	9.46	6.13	1.82	2.82	46.00	0.65	1.00	2.98	0.065
16H-2, 50–52	136.71	9.83	5.76	1.79	2.97	51.56	0.60	1.18	3.02	0.059
17H-2, 50–52	146.41	10.38	11.20	6.14	8.20	73.21	0.75	2.06	7.90	0.108
17H-5, 50–52	150.91	11.62	13.30	10.30	15.20	114.29	0.68	4.90	13.08	0.114
18H-2, 57–59	156.18	24.41	43.70	65.30	122.00	279.18	0.54	56.70	49.98	0.179
19H-2, 50–52	165.81	15.25	13.10	7.69	10.90	83.21	0.71	3.21	7.15	0.086
19H-5, 54–56	170.35	19.60	26.70	13.00	20.80	77.90	0.63	7.80	10.61	0.136
20H-2, 50–52	175.51	13.14	9.57	3.84	6.03	63.01	0.64	2.19	4.59	0.073
21H-2, 50–52	185.11	14.63	23.00	9.85	16.80	73.04	0.59	6.95	11.48	0.157
21H-5, 50–52	189.57	9.00	6.18	1.87	2.95	47.73	0.63	1.08	3.28	0.069

Table T9 (continued).

Core, section, interval (cm)	Depth (mbsf)	$\chi$ ( $10^{-8} \text{ m}^3/\text{kg}$ )	ARM ( $10^{-6} \text{ Am}^2/\text{kg}$ )	IRM@0.1T ( $10^{-4} \text{ Am}^2/\text{kg}$ )	IRM@0.9T ( $10^{-4} \text{ Am}^2/\text{kg}$ )	IRM@0.9T/ ARM	IRM@0.1T/ IRM@0.9T	IRM@0.9T- IRM@0.1T ( $10^{-4} \text{ Am}^2/\text{kg}$ )	IRM@0.9T/ $\chi$ ( $10^3 \text{ A/m}$ )	ARM/ $\chi$ ( $10^3 \text{ A/m}$ )
22H-2, 52–54	194.73	10.51	9.49	3.22	5.60	59.01	0.58	2.38	5.33	0.090
22H-5, 52–54	199.23	14.16	16.00	8.18	13.70	85.63	0.60	5.52	9.68	0.113
23H-2, 50–52	203.49	10.48	8.45	3.99	6.05	71.60	0.66	2.06	5.78	0.081
23H-5, 50–52	207.99	21.29	41.10	34.00	53.40	129.93	0.64	19.40	25.08	0.193
24H-2, 50–52	213.21	25.88	75.40	80.20	124.00	164.46	0.65	43.80	47.91	0.291
24H-5, 43–45	217.14	11.84	13.10	8.68	12.20	93.13	0.71	3.52	10.31	0.111
25H-2, 56–58	222.97	24.72	54.00	68.70	110.00	203.70	0.62	41.30	44.50	0.218
25H-5, 59–61	227.5	13.74	28.70	28.10	39.10	136.24	0.72	11.00	28.46	0.209
26H-2, 52–54	232.53	9.88	8.58	3.16	5.05	58.86	0.63	1.89	5.11	0.087
26H-5, 48–50	236.99	12.30	17.50	9.71	14.30	81.71	0.68	4.59	11.63	0.142
27H-2, 48–50	242.19	10.26	9.89	5.38	7.80	78.87	0.69	2.42	7.60	0.096
27H-6, 61–63	248.29	8.83	7.74	3.39	5.03	64.99	0.67	1.64	5.69	0.088
28H-2, 48–50	251.99	8.66	8.36	3.83	5.76	68.90	0.66	1.93	6.65	0.096
28H-5, 47–49	256.31	9.62	7.67	2.89	4.63	60.37	0.62	1.74	4.81	0.080